Published in final edited form as:
Sci Signal. 2019 November 12; 12(607): . doi:10.1126/scisignal.aay4430.

The ALK-1/SMAD/ATOH8 axis attenuates hypoxic responses and protects against the development of pulmonary arterial hypertension

Masato Morikawa[1,2,3], **Yoshihide Mitani**[4], **Katarina Holmborn**[5], **Taichi Kato**[4,10], **Daizo Koinuma**[1], **Junko Maruyama**[6,11], **Eleftheria Vasilaki**[2,3], **Hirofumi Sawada**[4,6], **Mai Kobayashi**[1], **Takayuki Ozawa**[1], **Yasuyuki Morishita**[1], **Yasumasa Bessho**[7,12], **Shingo Maeda**[8], **Johan Ledin**[5], **Hiroyuki Aburatani**[9], **Ryoichiro Kageyama**[7], **Kazuo Maruyama**[6], **Carl-Henrik Heldin**[2,3,*], **Kohei Miyazono**[1,2,3,*]

[1]Department of Molecular Pathology, Graduate School of Medicine, The University of Tokyo, Bunkyo-ku, Tokyo 113-0033, Japan

[2]Department of Medical Biochemistry and Microbiology, Science for Life Laboratory, Box 582, Biomedical Center, Uppsala University, SE-751 23 Uppsala, Sweden

[3]Ludwig Institute for Cancer Research, Science for Life Laboratory, Box 595, Biomedical Center, Uppsala University, SE-751 24 Uppsala, Sweden

[4]Department of Pediatrics, Mie University Graduate School of Medicine, Tsu, Mie 514-8507, Japan

[5]Genome Engineering Zebrafish Facility, Science For Life Laboratory, Uppsala University, SE-752 36 Uppsala, Sweden

[6]Department of Anesthesiology, Mie University Graduate School of Medicine, Tsu, Mie 514-8507, Japan

[7]Institute for Frontier Life and Medical Sciences, Kyoto University, Sakyo-ku, Kyoto 606-8507, Japan

[*]Correspondence should be addressed to: Carl-Henrik Heldin, Department of Medical Biochemistry and Microbiology, Box 582, Biomedical Center, Uppsala University, SE-751 23 Uppsala, Sweden, or Kohei Miyazono, Department of Molecular Pathology, Graduate School of Medicine, The University of Tokyo, 7-3-1 Hongo, Bunkyo-ku, Tokyo 113-0033, Japan. c-h.heldin@imbim.uu.se or miyazono@m.u-tokyo.ac.jp.

Author Contributions

M.M. conceptualized, designed and performed experiments, including retinal angiogenesis assay of *Atoh8*-deficient mice, interpreted results, prepared figures and wrote the manuscript. K.H., E.V. and J.L. performed zebrafish experiments. Y.B. and R.K. generated *Atoh8*-deficient mice, and Y. Mitani, T.K., J.M. and H.S. performed hemodynamic analysis. M.M and S.M. performed ISH of mice. M.M., D.K. and H.A. conducted microarray and ChIP-seq analysis. M.K. and T.O. helped to perform biochemical assays and mouse experiments, while Y. Morishita helped to perform histological analysis. K. Maruyama supervised the hemodynamic analysis. C.-H.H. and K. Miyazono coordinated all aspects of this work and wrote the manuscript.

Competing Interests

The authors declare that they have no competing interests.

Data and Materials Availability

All the supporting data for this study are available from the corresponding authors upon reasonable request. The microarray and ChIP-seq data in this publication have been submitted to the NCBI GEO database (https://www.ncbi.nlm.nih.gov/geo/) and assigned the identifier GSE104685.

Europe PMC Funders Author Manuscripts

[8]Department of Medical Joint Materials, Kagoshima University, Kagoshima, Kagoshima 890-8544, Japan

[9]Genome Science Division, Research Center for Advanced Science and Technology (RCAST), The University of Tokyo, Meguro-ku, Tokyo 153-8904, Japan

[10]Current address: Department of Pediatrics/Developmental Pediatrics, Nagoya University Graduate School of Medicine, Nagoya 466-8550, Japan

[11]Current address: Faculty of Medical Engineering, Suzuka University of Medical Science, Suzuka, Mie 510-0293, Japan

[12]Current address: Department of Systems Biology, Graduate School of Biological Sciences, Nara Institute of Science and Technology (NAIST), Ikoma, Nara 630-0101, Japan

Abstract

Dysregulated bone morphogenetic protein (BMP) signaling in endothelial cells (ECs) is implicated in vascular diseases such as pulmonary arterial hypertension (PAH). Here, we showed that the transcription factor ATOH8 was a direct target of SMAD1/5 and was induced in a manner dependent on BMP but independent of Notch, another critical signaling pathway in ECs. In zebrafish and mice, inactivation of *Atoh8* did not cause an arteriovenous malformation (AVM)-like phenotype, which may arise because of dysregulated Notch signaling. In contrast, *Atoh8*-deficient mice exhibited a phenotype mimicking PAH, which included increased pulmonary arterial pressure and right ventricular hypertrophy. Moreover, *ATOH8* expression was decreased in PAH patient lungs. We showed that in cells, ATOH8 interacted with hypoxia-inducible factor 2α (HIF-2α) and decreased its abundance, leading to reduced induction of HIF-2α target genes in response to hypoxia. Together, these findings suggest that the BMP receptor type II/ALK-1/SMAD/ATOH8 axis may attenuate hypoxic responses in ECs in the pulmonary circulation and may help to prevent the development of PAH.

Introduction

Dysregulated bone morphogenetic protein (BMP) signaling in endothelial cells (ECs) is implicated in vascular diseases (1–3). Mutations in *ENG, ACVRL1*, or *SMAD4* genes cause hereditary hemorrhagic telangiectasia (HHT), which is a multisystemic vascular disorder characterized by epistaxis, telangiectases, and arteriovenous malformations (AVMs). Mutations in *BMPR2, ACVRL1, ENG*, or *SMAD9* (the latter of which encodes the SMAD8 protein) underlie the pathogenesis of pulmonary arterial hypertension (PAH). The *BMPR2* gene encodes BMPRII, a type II receptor for BMP ligands, while the *ACVRL1* gene encodes an endothelial-specific type I receptor, ALK-1, whose ligands are transforming growth factor β (TGF-β), BMP-9 and BMP-10. The *ENG* gene encodes Endoglin (also known as CD105), a co-receptor for ALK-1. Receptor complexes containing ALK-1 phosphorylate BMP-specific receptor-regulated Smads (BR-SMADs). These consist of SMAD1, SMAD5, and SMAD8, which form heterotrimeric complexes with SMAD4. The SMAD complexes then translocate into the nucleus, where they bind to enhancers of target genes, such as *ID1* (which encodes inhibitor of differentiation-1 or inhibitor of DNA binding-1) (4). Therefore, the BMPRII/ALK-1/SMAD pathway in ECs is implicated in the

Europe PMC Funders Author Manuscripts

pathogenesis of both HHT and PAH, although the molecular mechanisms involved in the two diseases remain elusive.

Accumulating in vitro and in vivo observations indicate that ALK-1/SMAD signaling in ECs induces several Notch target genes, such as *HEY1, HEY2*, and *HES1*, independently of canonical Notch activation (5, 6). ID1, HEY1/2, and HES1 belong to the basic helix-loop-helix (bHLH) transcription factor superfamily (7), but because it lacks a DNA-binding basic region, ID1 functions as a dominant-negative regulator for other bHLH transcription factors. In cultured ECs, ID1 stimulates EC migration and tube formation (8). In contrast, interaction among ID1, HEY1/2 and HES1 exerts both synergistic and antagonistic effects, suggesting that the relative abundance of these proteins may affect the outcome in a context-dependent manner (1). Thus, it is possible that the bHLH regulatory network regulated by BMP and/or Notch plays important roles in the development of vascular lesions in HHT and PAH (9).

In PAH, endothelial dysfunction plays a central role in the initiation and progression of the disease, although dysfunction of smooth muscle cells and circulating mononuclear cells are also implicated in the pathogenesis of this disease (10, 11). Consistently, mice with endothelial-specific deletion of *Bmpr2* or *Smad1* have phenotypes reminiscent of the symptoms of PAH, such as elevated pulmonary arterial pressure and right ventricular hypertrophy, which accompany milder histological changes compared with rat PAH models (12–14). In addition, activation of BMPRII by administration of FK506 or activation of ALK-1 by stimulation with BMP-9 partially restores the phenotype (15, 16), suggesting that PAH is caused, or at least modulated, by deficient BMPRII/ALK-1/SMAD signaling in ECs. Although the precise nature of the endothelial dysfunction in the pathogenesis of PAH has not been determined, several groups have pointed out that BMP protects ECs against apoptosis (14, 16–18).

In this study, we showed that a bHLH protein, ATOH8, was a direct target of SMAD1/5, which is induced in a BMP-9/ALK-1/SMAD-dependent and Notch-independent manner. Inactivation of *Atoh8* did not induce AVMs. Instead, mice lacking *Atoh8* (also known as *Math6* (19)) developed a phenotype resembling PAH, a BMP-related vascular disease. In pursuing a mechanism, we discovered that ATOH8 bound to hypoxia-inducible factor (HIF)-2α and decreased its abundance. Forced expression of ATOH8 attenuated HIF-2α protein stabilization and target gene induction in response to hypoxia. Overall, our findings reveal important insights into the pathogenesis of PAH, in which the BMPRII/ALK-1/SMAD/ATOH8 axis counteracts hypoxia-induced HIF-2α activation.

Results

ATOH8 is a bHLH transcription factor induced by BMP, but not by Notch in ECs

To begin to probe the possible involvement of the BMPRII/ALK-1/SMAD pathway and the Notch pathway in the pathogenesis of HHT and PAH, we compared a set of BMP-9/ALK-1 direct target genes (5) and sets of genes induced by the Notch ligand DLL4 or the Notch intracellular domain (NICD) in human umbilical vein endothelial cells (HUVECs) (20, 21). Among 70 putative direct target genes of ALK-1, 8 genes (11.4%), including *HES1, HEY1, HEY2* and *JAG1*, were also targets of Notch signaling in HUVECs (Fig. 1A). On the other

hand, we found that the bHLH transcription factor ATOH8 (19) was induced by BMP, but not by Notch (Fig. 1B, and Data File S1). We then utilized a mouse enhancer database validated by reporter assays in transgenic mice in vivo (VISTA Enhancer Browser) (22), to evaluate the SMAD1/5 binding regions. Among 259 enhancers related to blood vessels or the heart, 18 enhancers were bound by SMAD1/5 (Data File S2). The enhancer mm123 in the *Atoh8* gene locus showed positive in vivo enhancer activity in E11.5 embryonic heart (Fig. 1C and Data File S2), suggesting a potential role of ATOH8 in the cardiovascular system. *ATOH8* mRNA was expressed in the vasculature of E17.5 embryonic lung, but not in the heart (Fig. 1D).

The *ATOH8* gene encodes a bHLH transcription factor (19). *ATOH8* is induced not only by BMP-9 acting through ALK-1, but also by BMP-6 which activates SMAD1/5/8 mainly through ALK-2 in ECs (5), whereas other pro-angiogenic cytokines, such as vascular endothelial growth factor (VEGF), basic fibroblast growth factor (bFGF), or TGF-β, did not induce *ATOH8* mRNA (Fig. 2A). BMP-9 induced *ATOH8* mRNA as early as 1 h after stimulation (Fig. 2B). Loss-of-function of the common mediator SMAD4 is a well-established way to determine whether a target gene is controlled by the SMAD pathway. Similar to *ID1,* the induction of *ATOH8* was inhibited in SMAD4-depleted cells, indicating that the induction depended on canonical SMAD signaling (Fig. 2C and 2D). On the other hand, *ATOH8* was not induced by NICD overexpression (Fig. 2E). We also confirmed the presence of endogenous ATOH8 in the nuclear fraction of HUVECs treated with BMP-9 (Fig. 2F). These results confirm the notion that ATOH8 is a direct target of ALK-1/SMAD signaling in ECs. The mRNAs encoding other Atonal-family members were neither expressed nor induced by BMP-9 in HUVECs, based on our expression microarray data (5) (fig. S1A).

There are two SMAD1/5 binding regions (SBR) in the *ATOH8* gene locus: at 10 kb upstream of the transcription start site (TSS) and in the second intron, both of which are well conserved from zebrafish to human (Fig. 1C and 2G). In addition, a SMAD1/5 binding motif, or GC-SBE (5), is also conserved from zebrafish to human (fig. S1B). To investigate whether the SBRs serve as enhancers, each fragment was subcloned into a luciferase reporter construct (fig. S1C) and was introduced into HUVECs using a lentiviral vector system. BMP-9 activated these reporters in HUVECs in a dose-dependent manner (Fig. 2H), demonstrating that these fragments functioned as transcriptional enhancers. This result was reproduced in a transfectable mouse pancreatic islet microvascular endothelial cell line, MS1 (fig. S1D). In addition, mutations in these motifs, GGCGTC to GataTC for SBR1 and GGCGCC to GaattC for SBR2 (fig. S1B), resulted in significant attenuation of BMP responsiveness (Fig. 2H and fig. S1D). These findings showed that the ALK-1/SMAD pathway directly induces *ATOH8* gene expression through its enhancers.

Because ATOH8 is a member of the bHLH transcription factor superfamily, which play a role during endothelial lineage commitment (23), we explored the possibility that ATOH8 participates in the bHLH regulatory network, which may determine tip cell and stalk cell phenotypes. However, microarray gene expression profiling with both gain-of-function (GOF) and loss-of-function (LOF) of ATOH8 revealed that ATOH8 did not influence tip cell or stalk cell decisions; *HEY1*, a stalk-cell-enriched gene, was induced by ATOH8

consistently in either GOF and LOF models, whereas another stalk-cell-enriched gene, *FLT1* (also known as *VEGFR1*), was repressed (fig. S1E). For tip-cell-enriched genes, such as *DLL4, PDGFB, KDR* (also known as *VEGFR2*) and *FLT4* (also known as *VEGFR3*), we did not see any specific trends (fig. S1E). This finding is in contrast to the effects of overexpression of ID proteins and HEY1/2, which cause a decrease in tip-cell-enriched transcripts, such as *DLL4, KDR* and *FLT4* (6). Moreover, gene set enrichment analysis (GSEA) revealed that the expression of ATOH8 was strongly associated with E2F, Myc, hypoxia, and epithelial-to-mesenchymal transition (EMT) (fig. S1F and S1G). Thus, our observations suggest that ATOH8 functions in a different manner compared to other bHLH proteins.

Zebrafish *atoh8* is expressed in large vessels but *atoh8* knockout fish display normal vascular patterning

Because the SMAD1/5 binding regions are well conserved from zebrafish to human, we first used zebrafish (*Danio rerio*) as an in vivo model system (Fig. 1C and S1B). We investigated the expression of the zebrafish *atoh8* mRNA during development using whole-mount in situ hybridization (ISH) with three different probes (fig. S2A). *Z*ebrafish *atoh8* was expressed in large vessels, pectoral fins, heart, and the caudal hematopoietic tail region, consistent with previous studies (23–25) (Fig. 3A and fig. S2B). Intriguingly, these regions have high activity of BMP signaling (26, 27), suggesting that *atoh8* could be a target of BMP signaling in zebrafish.

We then assessed sprouting of intersegmental vessels (ISVs) of transgenic fish Tg(*fli:EGFP*) (28) in which the vascular endothelium was visualized by EGFP expression. We injected morpholinos that blocked either splicing or translation (Trl) of the *atoh8* transcript. *atoh8* morphants had normal vascular patterning, with a trend of slight delay in formation of the ISVs and dorsal longitudinal anastomotic vessels (DLAVs) (fig. S2C). We then generated 2 mutant lines designated $atoh8^{uu3111}$ and $atoh8^{uu3112}$ using CRISPR/Cas9 (Fig. 3B). Each line had a small deletion with a frame-shift in Exon 1, resulting in loss of the bHLH domain of ATOH8 protein (Fig. 3B and 3C). Consistent with a report (24), loss of function of *atoh8* did not affect normal vascular patterning under standard laboratory conditions (Fig. 3D). This finding indicated that loss-of-function of *atoh8* did not affect Notch signaling, dysregulation of which accompanies AVM formation or excessive sprouting of zebrafish (29). To further characterize the vascular phenotype, we used a Vertebrate Automated Screening Technology (VAST) BioImager platform (30), which enables precise handling of larvae and obtaining standardized images. However, we were not able to detect differences in ISV angiogenesis between WT and *atoh8* knockout fishes (Fig. 3D and 3E). Because our mRNA expression profile obtained by ISH (Fig. 1D and 3A) suggested a potential role of ATOH8 in vascular biology, we decided to use a mouse model to evaluate whether the gene is implicated in the pathogenesis of the BMP-related genetic vascular diseases.

Atoh8-deficient mice have elevated pulmonary arterial pressure

We generated *Atoh8*-deficient mice by replacing most of the coding region of exon 1 with a *LacZ* reporter cassette, hereafter referred to as $Atoh8^{LacZ(ex1)}$ or $Atoh8^{-}$ (Fig. 4A). Several lines of knockout mice lacking *Atoh8* have been reported: deletion of exons 1 and 2 together

with the intervening intron of *Atoh8* (31), and deletion of either exon 1 or exon 2 (25). Similar to previous results (25), *Atoh8*$^{-/-}$ mice were viable and present at the expected Mendelian ratio (fig. S3A). Although there was no obvious increase of unexpected death in *Atoh8*$^{-/-}$, the body size of *Atoh8*$^{-/-}$ mice was smaller than that of heterozygous and wild-type (WT) littermates (fig. S3B and S3C). To investigate roles of ATOH8 in angiogenesis during vascular development, the retinal vasculature of post-natal day 5 (P5) neonates was analyzed. *Atoh8*$^{-/-}$ mice showed a delay in the radial outgrowth of retinal vasculature (Fig. 4B and 4C). However, we could not detect excessive sprouting or AVMs in the retina, which are observed in mice with endothelium-specific and inducible inactivation of ALK-1 (32).

We then explored whether deletion of the *Atoh8* gene might cause a phenotype resembling human PAH. ISH showed that *Atoh8* mRNA in lung ECs in adult mice maintained in normoxia or hypoxia (Fig. 5A and fig. S4A). Because pathological changes spontaneously develop in older *Bmpr2*$^{+/R899X}$ and *Smad9*$^{-/-}$ mice at 6 months (16) and 11.5 months of age (33), respectively, *Atoh8*$^{-/-}$ male mice at 5 to 8 months of age were evaluated. The right ventricular systolic pressure (RVSP) of *Atoh8*$^{-/-}$ male mice was significantly elevated compared to that of *Atoh8*$^{+/+}$ littermates, whereas the systemic systolic blood pressure (SBP) was not changed (Fig. 5B and fig. S4B). Moreover, hypoxic conditions exacerbated the phenotype; the RVSP of *Atoh8*$^{-/-}$ male mice maintained under hypoxic conditions was higher than that of *Atoh8*$^{+/+}$ littermates, although *Atoh8*$^{-/-}$ had lower systemic SBP (Fig. 5C). We detected PAH-like pathological changes, such as an increase in Fulton index (RV/(LV+S)) and coverage of peripheral small arteries in the lung by SMA-positive cells without obvious AVM formation or differences in vascular density in the lung (Fig. 5D-5G and fig. S4C). *Atoh8*$^{+/-}$ mice had tachycardia under normoxic conditions and lowered blood pressure under hypoxic conditions (Fig. 5B,5C and fig. S4B), which can be explained by overloading of the right ventricle. These findings suggest that *Atoh8*-deficient mice exhibited a PAH-like phenotype, similar to mice with dysregulated BMPRII/ALK-1/SMAD pathway (14, 16).

To confirm the potential relevance of ATOH8 in human PAH, we reanalyzed a microarray data set derived from PAH patients, which contains probe sets for *ATOH8* (Fig. 5H). As previously reported, the gene encoding cytochrome P450 7B1 (*CYP7B1*) was highly expressed in the PAH lung (34). Intriguingly, *ATOH8* was expressed at significantly lower levels in the PAH lung compared with the healthy control (Fig. 5H). Together, these data suggest a potential role of the ALK-1/SMAD/ATOH8 axis in the development and disease progression of PAH.

ATOH8 physically interacts with HIF-2α and decreases its abundance

To gain further insights into the roles of ATOH8 in PAH, and to avoid possible phenotypic differences among ECs, we used human pulmonary arterial endothelial cells (HPAECs), in addition to HUVECs. Although there are cell-type-specific SMAD1/5 binding sites in each ECs, around 40% of binding sites were shared between HUVECs and HPAECs (Fig. 6A). *ATOH8* was a common ALK-1/SMAD target gene in HPAECs (Fig. 6B and 6C). We also performed chromatin immunoprecipitation-sequencing (ChIP-seq) in HPAECs stably expressing FLAG-ATOH8. In the *ATOH8* gene locus, FLAG-ATOH8 bound to the SBR2

region (Fig. 1C and 6B). However, the number of binding sites of ATOH8 was around 100 in the whole genome (Data File S3). Although ChIP analysis with stably expressed protein can sometimes cause non-specific binding, the enrichment of an E-box motif, a motif for bHLHs, in the FLAG-ATOH8 binding sites (Fig. 6D) argues against the possibility that the binding represents non-specific binding of overexpressed FLAG-ATOH8. In addition, we found that the half-life of ATOH8 was about 30 min (Fig. 6E). ATOH8 without the bHLH region (ATOH8 Δ231-286) was more stable than wild-type protein (Fig. 6F and fig. S5A), suggesting that ATOH8 exerts its function through protein-protein interaction through the HLH domain and that this interaction affects the stability of ATOH8 and its binding partner. These data suggest that the role of ATOH8 as a DNA-binding factor is minor in cultured ECs, which is consistent with the low number of FLAG-ATOH8 binding sites in the genome.

We then explored a functional interaction between ATOH8 and hypoxia, because the PAH-like phenotype observed in *Atoh8*-deficient mice was exacerbated in response to hypoxia. The results of GSEA analysis in HUVECs indicated a significant enrichment of hypoxia-associated genes among the genes induced by ATOH8 (fig. S1G). Because another bHLH protein, BHLHE41 (also known as DEC2 or SHARP1), promotes the proteasomal degradation of HIF-1α (35), we assessed the possibility that ATOH8 has a similar effect. We found that ATOH8 formed a complex with both HIF-1α and HIF-2α, but not with HIF-1β in HEK293T cells (Fig. 7A). The protein abundance of HIF-1α and HIF-2α was decreased by co-expression of ATOH8 (Fig. 7B and fig. S5B), but not by co-expression of another BMP-9/ALK-1 target bHLH protein, HEY1 (Fig. 1A) (5, 6). The destabilization of HIF-2α was rescued by the proteasome inhibitor MG132 (Fig. 7C). Using ATOH8 mutants, we found that the bHLH domain of ATOH8 was necessary and sufficient to induce degradation of HIF-1α and HIF-2α (Fig. 7D and fig. S5C). Moreover, an ATOH8 fragment consisting of amino acid residues 241-289 also destabilized HIF-1α and HIF-2α (Fig. 7D and fig. S5C), indicating that the basic region was not required. Consistently, ATOH8 lacking the bHLH region had a weaker affinity for HIF-2α (Fig. 7E). Although our ATOH8 antibody was not suitable for co-immunoprecipitation experiments, endogenous HIF-2α was co-precipitated with FLAG-ATOH8 in FLAG-ATOH8 stably-expressing HPAECs (Fig. 7F).

ATOH8 attenuates hypoxia-induced HIF-2α activation and target gene expression

In HPAECs cultured under hypoxic conditions, adenovirally overexpressed ATOH8 attenuated the induction of HIF-1α and HIF-2α proteins and suppressed hypoxia-mediated induction of the endothelial HIF-2α-selective target genes *DLL4* and *ANGPT2* (36, 37) (Fig. 8A and 8B). On the other hand, the HIF-1α-selective target genes *VEGFA* and *PGK1* were not affected by the forced expression of ATOH8. Consistently, knock-down of ATOH8 by siRNA in HPAECs led to enhanced expression of *DLL4* and *ANGPT2* without affecting the expression of *VEGFA* and *PGK1* (Fig. 8C). Moreover, in our experimental conditions, the number of cells cultured under hypoxia was lower than those cultured in normoxia. Both BMP-9 treatment and transient ATOH8 overexpression rescued the decrease of cell number during 48 h hypoxia (Fig. 8D). Thus, out data showed that ATOH8 counteracts hypoxia-mediated induction of HIF-2α target genes in ECs and hypoxia-induced cellular response.

Discussion

BMP modulates several biological processes of ECs, such as apoptosis, mitochondrial dysfunction and inflammation, which result in the initiation and progression of PAH (1, 2, 10, 11). However, it still remains unclear how the mutations that cause the disease seem to be restricted to the pulmonary circulation and show variable penetrance. One explanation may be the characteristics of the pulmonary circulation: Deoxygenated blood travels through the right atrium, right ventricle, and pulmonary artery for gas exchange. The main source of BMP-9 and BMP-10 is the liver and the heart, respectively (1, 2), and BMP-10 expression in particular is restricted to the right atrium in adult (38). Thus, the pulmonary circulation is close to the sources of the circulating ALK-1 ligands, which would enable these ligands to maintain the normal physiology of pulmonary arterial ECs. On the other hand, pulmonary arterial ECs are exposed to lower oxygen tension compared with arterial ECs in other organs. Accordingly, several groups have reported that the development of PAH depends on HIF (39, 40). Intriguingly, HIF-1α and HIF-2α are not redundant in ECs, and HIF-2α plays essential roles in the pathogenesis of PAH at least in animal models (39, 40). Inactivation of the oxygen sensor prolyl-4 hydroxylase 2 (PHD2) in ECs causes PAH through HIF-2α (41, 42). Moreover, translational repression of HIF-2α also protects against PAH development (43). Thus, it is possible that HIF-2α (encoded by *EPAS1*) is the dominant HIFα subunit in ECs that is associated with the PAH phenotype. We showed that ATOH8 decreased the abundance of both HIF-1α and HIF-2α and antagonized hypoxia-mediated induction of HIF-2α-selective target genes, such as *DLL4* and *ANGPT2* (36, 37) but not that of HIF-1α-selective targets (Fig. 8B and 8C). These differential effects may be caused by relative abundance of the HIF proteins and different threshold for the target gene induction. Together, we conclude that the BMPRII/ALK-1/SMAD/ATOH8 axis suppresses HIF-2α protein abundance in ECs and protects against PAH development.

ATOH8 was originally isolated as a bHLH transcription factor in the *Drosophila ato* (*atonal*) family (19). The *Drosophila* ortholog of *ATOH8, net* (FlyBase ID: FBgn0002931) is associated with regulation of wing veins and intervein patterning (44). In vertebrates, variable phenotypes have been reported in zebrafish (23–25, 45) and mice (25, 31). However, using zebrafish *atoh8*^{sa1465} allele which encodes a truncated protein ATOH8-K100X lacking the entire bHLH domain, Place and Smith concluded that loss of *atoh8* does not affect normal vascular patterning (24). We also could not detect defects in ISV angiogenesis in our *atoh8* knockout fishes under standard laboratory conditions (Fig. 3D and 3E). On the other hand, we found that *Atoh8*$^{-/-}$ mice have increased RVSP without changes in SBP (Fig. 5B and 5C), suggesting that the elevated RVSP is not the result of left ventricular dysfunction or defects in other organs, such as the kidney. Together with *Atoh8* mRNA expression profiles (Fig. 5A), we conclude that loss-of-function of *Atoh8* of the ECs in the lung is implicated in the pathogenesis of the PAH. Although the Fulton index was increased in *Atoh8*$^{-/-}$ mice (Fig. 5D), the right ventricle of *Atoh8*$^{-/-}$ was dilated rather than hypertrophic (Fig. 5E). It is possible that the BMP/SMAD/ATOH8 axis in cardiomyocytes affects the remodeling response, because cardiac hypertrophy induced in a mouse model of pressure overload is attenuated by treatment with the BMP type I receptor kinase inhibitor DMH1 (46).

In addition, the body size of our *Atoh8*$^{-/-}$ mice was smaller than that of heterozygous and WT littermates (fig. S3B and S3C). Although disrupted angiogenesis may explain the smaller body size, it is also possible that ATOH8-HIF interaction can also play roles in skeletal bone formation and/or nutrient metabolism, affecting systemic development. Notably, ATOH8 has been implicated in hepatic iron metabolism (47), which can also be regulated by hypoxia. Further work is needed to elucidate the detailed role of ATOH8 in hypoxia.

In this work, we found that ATOH8 interacts with both HIF-1α and HIF-2α. Montagner *et al.* reported that BHLHE41 interacts with the 20S proteasomal subunit α4 (the protein name is based on a systematic nomenclature (48); the official gene symbol is *PSMA7*, or subunit alpha type 7), and facilitates the interaction between HIF-1α and PSMA7 (35). A BHLHE41 mutant lacking the bHLH domain interacted with HIF-1α but not with PSMA7 (35). On the other hand, we showed that the HLH domain of ATOH8 was necessary and sufficient for interaction with and degradation of HIF-1α/-2α. This interaction might be a potential therapeutic target to antagonize HIF function. A selective HIF-2α antagonist PT2399, which targets the HIF-2α/HIF-1β interaction through the bHLH-PAS domains (49) and degrades HIF-2α protein, has been developed and is effective for treatment of renal cell carcinoma (50, 51). Our data suggest that ATOH8 is an endogenous antagonist against at least HIF-2α, and that application of a HIF-2α antagonist could be a treatment option for PAH especially at the early phase of the disease progression.

In summary, we have unraveled potential roles of ATOH8 in the pathogenesis of PAH. Our findings indicate that ATOH8 attenuates HIF-2α activation and target gene expression, supporting the notion that dysregulation of ATOH8 in BMP signaling causes endothelial dysfunction, promoting hypoxia-induced initiation and progression of PAH.

Materials and Methods

Cell culture

HEK293T and MS1 cells were obtained from the American Type Culture Collection (ATCC). HEK293A and HEK293FT were obtained from Invitrogen (Thermo Fisher Scientific, Waltham, MA, USA). Human Umbilical Vein Endothelial Cells (HUVECs) and Human Pulmonary Artery Endothelial Cells (HPAECs) were obtained from Lonza (Thermo Fisher Scientific). The endothelial cells were used at passage number 4-8 in all experiments. HEK293T, HEK293FT and HEK293A cells were maintained in Dulbecco's modified Eagle's medium (Gibco, Thermo Fisher Scientific), supplemented with 10% (v/v) fetal bovine serum (FBS) (HyClone, GE Healthcare Life Sciences, Piscataway, NJ, USA) and 100 U/ml penicillin-streptomycin (Gibco, Thermo Fisher Scientific). HUVECs and HPAECs were cultured in EBM-2 endothelial basal medium with EGM-2 BulletKit supplement, containing 2% (v/v) FBS and growth factors (Lonza, Thermo Fisher Scientific). For ligand treatment, cells were seeded 48 h before treatment in media containing serum, unless otherwise indicated. Cell culture under hypoxic conditions (≤1% O_2 and 5% CO_2) was carried out using the AnaeroPack-Kenki 5% system (Mitsubishi Gas Chemical, Tokyo, Japan). Cells were counted using an automated cell counter (TC20, Bio-Rad, Hercules, CA, USA). For cell counting after 48 h of hypoxia, HPAECs were seeded in a 6-well plate at a cell density

of 2×10^4 cells per well 24 h before treatment. After the medium was changed with 2× diluted EGM-2 (1% serum) medium, cells were treated with BMP-9 (5 ng ml^{-1}) or infected with either Ad-ATOH8 or control (Ad-LacZ) for 24 h. Cells were then transferred to hypoxic (≤1% O_2) or normal (21% O_2) conditions for an additional 48 h without medium change. Cultured cells were routinely tested for mycoplasma contamination using e-Myco VALid-Q mycoplasma qPCR detection kit (iNtRON Biotechnology, Korea).

Reagents and antibodies

Recombinant human BMP-6, BMP-9, VEGF, bFGF and TGF-β were purchased from R&D Systems (R&D Systems, Bio-Techne, Minneapolis, MN, USA). Cycloheximide (CHX) was purchased from Sigma-Aldrich (Merck, Darmstadt, Germany), and MG132 was from Peptide Institute (Osaka, Japan). The following antibodies were used: anti-FLAG M2 (F3165; Sigma-Aldrich, Merck), anti-DDDDK (PM020; MBL, Tokyo, Japan) which recognizes the FLAG epitope, anti-Myc, anti-HA (HA124; Nacalai Tesque, Kyoto, Japan), anti-HA (#561; MBL), anti-α-tubulin (AC-15; Sigma-Aldrich, Merck), anti-SMAD1 (913C1b; Bio Matrix Research, Chiba, Japan) which recognizes both SMAD1 and SMAD5 for ChIP assays (5), anti-phospho-SMAD1/5/8 (Cell Signaling Technology, Danvers, MA, USA), anti-PECAM1 (clone 18; BD bioscience, San Jose, CA, USA), anti-HIF-1α (NB100-449, Novus Biologicals, Bio-Techne), anti-HIF-2α (NB100-122, Novus Biologicals, Bio-Techne), anti-α-smooth muscle actin (clone 1A4; Sigma-Aldrich, Merck), and anti-HDAC1 (clone 2E10, #05-100; Millipore, Merck). A rabbit polyclonal anti-ATOH8 antibody was raised against residues 306-321 of human ATOH8, CTRTLQAEGRAKKRKE.

Plasmid construction

The coding region of the human *ATOH8* (GeneBank accession NM_032827.5), *HEY1* (NM_012258.3), *BHLHE41* (NM_030762.2), *HIF1A* (NM_001530.3), *EPAS1* (NM_001430.4), *ARNT* (NM_001668.3), and *VHL* (NM_000551.3) genes were amplified by PCR and were subcloned into the pcDEF3-FLAG, 3×FLAG, 6×Myc, and HA vectors (52). Deletion mutants were generated using PCR with specific primers with sites for restriction enzymes with/without stop codon. Full-length cDNA for the zebrafish *atoh8* gene (IMAGE clone ID: 7056816) in an expression vector pSport6.1 was purchased from Open Biosystems (GE Healthcare Life Sciences). Notch1 intracellular domain (NICD)-Myc construct was kindly provided by Dr. S. Chiba (Tsukuba University, Japan). FLAG-tagged ATOH8 cDNA was cloned into the CSII-EF-RfA lentiviral vector (a gift from Dr. H. Miyoshi, RIKEN, Japan; present address, Keio University, Japan). Each fragment of SMAD1/5 binding regions was amplified from human genomic DNA by PCR, cloned into a modified pGL4.10 reporter plasmid (Promega, Fitchburg, WI, USA) driven by minimal adenoviral major late promoter (MLP), essentially as described previously (5). A point mutation was introduced by site-directed mutagenesis using PCR with specific primers. pGL4 constructs were subcloned between *EcoR*I and *Xho*I sites of the lentiviral vector construct CS-CDF-CG-PRE. All sequences were confirmed by Sanger sequencing analysis.

Zebrafish lines and maintenance

Zebrafish (*Danio rerio*) were maintained according to standard protocols. The following zebrafish strains were used: wild-type AB and WIK, and the transgenic line Tg(*fli1*:*EGFP*)

(28). Images were obtained with a Nikon SMZ1500 fluorescence microscope (Nikon, Tokyo, Japan) (53). All zebrafish experiments were carried out in compliance with the guidelines at Genome Engineering Zebrafish Facility, Science for Life Laboratory, Uppsala University.

Generation of *atoh8* knockout zebrafish and vascular phenotype screening

Generation of *atoh8* knockout fish lines using the CRISPR/Cas9 technique was performed as described previously (54). Briefly, guide RNA (gRNA) was designed to target the first exon of *atoh8* gene (GGGAGCGCGCGGAGTCGCCT; see Fig. 3B), with 5'-terminal modification (GG) for transcription with T7 polymerase during gRNA synthesis. Each founder (F_0) was outcrossed with Tg(*fli1*:*EGFP*). Heterozygous F_1 adults with *fli1*:*EGFP* were screened, and 2 mutant lines designated *atoh8*^{uu3111} and *atoh8*^{uu3112} were confirmed (Fig. 3B and 3C). The heterozygous F_1 fishes were incrossed and the resulting progenies (F_2) were analyzed blindly and genotyped afterward. For detailed analysis of the vascular phenotype, we utilized the VAST BioImager platform (30) (Union Biometrica, Boston, MA, USA) according to the manufacturer's instructions. ISV formation was quantified in the trunk region posterior to the end of yolk extension.

Zebrafish whole mount in situ hybridization and morpholino experiments

Whole-mount in situ hybridization was performed essentially as described previously (55). The pSport6.1-atoh8 plasmid was linearized with KpnI and NdeI and transcribed in vitro by T7 RNA polymerase with digoxigenin labeling mixes (Roche Life Science, Indianapolis, IN, USA) for the antisense *atoh8* RNA probe, 1.2 kb and 0.6 kb of the 3' region, respectively (see also fig. S2A). To generate a 5' non-overlapping antisense probe, full-length *atoh8* cDNA was digested with KpnI and *atoh8* (1-845) was subcloned into a pcDNA3 vector (Invitrogen, Thermo Fisher Scientific), which was linearized with EcoRI and transcribed in vitro by T7 RNA polymerase. To generate sense probe as a negative control, the pcDNA3-*atoh8*(1-607) was linearized with HindIII, and transcribed by Sp6 RNA polymerase (Roche Applied Science). After hybridization, probes were detected using the BM Purple AP Substrate precipitating solution (Roche Applied Science) according to the manufacturer's recommendations.

To eliminate *atoh8* function, two types of antisense morpholino oligonucleotide were used to disrupt the translation of *atoh8* transcripts. The translation-blocking morpholino, 5'-TTAGATGTGGGTTCTTCATTTCGGA-3' and the splice blocking one, 5'-GTACCTGTAAAAGTAGATCAAAGGG-3' (45), were designed and synthesized by Gene Tools (Philomath, OR, USA).

Mouse experiments

Atoh8 mutant mice in C57BL/6J background were generated as follows (see also Fig. 4A): Part of exon 1 of *Atoh8*, including the initiating methionine codon, was deleted and replaced with a cassette encoding IRES-*lacZ* and neomycin resistance. *Atoh8* mutant mice were backcrossed onto C57BL/6 mice (Japan SLC, Shizuoka, Japan) for at least 12 generations. We used WT or heterozygous littermates as control. All mouse experiments were reviewed and approved by the Animal Ethics Committees of The University of Tokyo, Mie University,

Kyoto University and Kagoshima University, and performed in accordance with the institutional guidelines.

Genotypes were determined by Southern blotting or PCR. For PCR analysis, the WT Atoh8 allele was detected using a forward primer (primer 1; 5'- GCT CAG CGC GGC GGC CAC CCG GCA CAG CCA -3') and a WT reverse primer (primer 2; 5'- GCA CCG GCT CCT TGC CTT TCC GCT TGA GCT -3'). This primer pair amplified a 211 bp fragment from the WT allele. To detect the mutant allele, we used a forward primer (primer 1) and a mutant-allele reverse primer (primer 3; 5'- GTT CCG CTG CCT GCA AAG GGT CGC TAC AGA -3'). In this case, a 405 bp fragment was detected in mice heterozygous or homozygous for the mutant Atoh8 allele, while no signal was detected in WT mice.

P5 mouse eyes were enucleated and fixed for 20 min in 4% paraformaldehyde (PFA) in PBS at room temperature (RT). Retinas were dissected and postfixed overnight in 4% PFA in PBS at 4°C. Retinas were then blocked in blocking buffer (Blocking One, Nacalai Tesque) followed by incubation with primary antibodies in the blocking buffer. ECs were visualized with rat monoclonal anti-PECAM1 antibody. Alexa 488-conjugated secondary antibody was from Molecular Probes (Invitrogen, Thermo Fisher Scientific). Images were obtained with a Zeiss LSM 510 Meta confocal microscope (Carl Zeiss Microscopy, Jena, Germany). Vessel lengths, branching points and junctional density were analyzed using AngioTool (56).

For measurement of systemic blood pressure and right ventricular pressure, we analyzed aged male mice (5–8 months of age) housed in room air, or housed in hypobaric chambers (380 mmHg, equivalent to 10% normobaric oxygen at sea level) for 3 weeks. Systemic blood pressures and heart rates were measured in awake mice by the tail-cuff method (BP-98A, Softron, Tokyo, Japan). Mice were anesthetized with an intraperitoneal injection of pentobarbital (50 mg/kg). Subsequently, a 27-gauge needle connected to a pressure transducer was inserted into the right ventricle through a subxyphoid puncture. Right ventricular pressure was recorded using an amplifier system (AP620G, Nihon Kohden, Tokyo, Japan) and a monitor (polygraph system, Nihon Kohden). Mice were then sacrificed and the hearts and lungs were harvested. The Fulton index was calculated by measuring the dry weight of the right ventricle relative to the left ventricle and the septum (RV/(LV+S)). The left lung was fixed in 4% PFA in PBS, followed by dehydration and paraffin embedding. Tissue sections were examined using a BZ-X710 microscope (Keyence, Osaka, Japan). Peripheral pulmonary arteries ranging from 25 to 75 μm in size in the lower 2/3 of left lung were marked and counted in a blind manner.

In situ hybridization (ISH)

In situ hybridization (ISH) of formalin-fixed paraffin-embedded tissues was performed using RNAscope 2.5 HD Reagent Kit-RED (#322350, Advanced Cell Diagnostics, Bio-Techne), according to the manufacturer's instructions. Mouse *Atoh8* mRNA was detected using a specific probe against Mm-Atoh8 (NM_153778.3) (#457501, Advanced Cell Diagnostics). Probes against a housekeeping gene peptidylprolyl isomerase B (*Ppib*) (#313911, Advanced Cell Diagnostics) and bacterial gene *DapB* (#310043, Advanced Cell Diagnostics) were used as positive and negative controls, respectively.

RNA isolation, quantitative real-time reverse transcription-PCR (qRT-PCR)

Extraction of total RNA and qRT-PCR were performed as described (5). qRT-PCR was performed in the Applied Biosystems 7500 Fast Real-Time PCR System or StepOnePlus Real-Time PCR Systems (Applied Biosystems, Thermo Fisher Scientific). Relative quantification was performed using the ΔΔCt method, and the data were normalized with *GAPDH* or *HPRT1* (hypoxic condition). Primer sequences are given in Data File S4.

Adenovirus production

Adenoviruses encoding lacZ (β-galactosidase), ATOH8, and NICD were generated as reported previously (57). Virus production and amplification were performed in HEK293A cells, and purified using the Adenovirus Standard Purification ViraKit (Virapur, San Diego, CA, USA). The multiplicity of infection (MOI) used in the current study was 100.

Lentivirus production

Recombinant lentiviruses were produced by transient transfection using Lipofectamine 2000 (Invitrogen, Thermo Fisher Scientific) in HEK293T cells or HEK293FT cells, and were concentrated using the Lenti-X Concentrator (Clontech, TaKaRa Bio, Shiga, Japan).

Luciferase assays

Because transfection efficacy is very low in HUVECs and transfection is rather toxic, we adapted lentiviral expression system essentially as described previously (5). Cells stably expressing the reporter plasmid were stimulated with indicated doses of BMP-9 and were then harvested and assayed for luciferase activity at 12 h after stimulation. Luciferase activities of the cell lysates were determined using a part of the Dual-luciferase Reporter Assay System (Promega).

For MS1 cells, transient transfection was carried out using Lipofectamine 2000 (Invitrogen, Thermo Fisher Scientific), according to the manufacturer's instructions. Cells were transiently transfected with 1 μg of the luciferase-reporter constructs along with 0.1 μg of Renilla luciferase reporter vector pGL4.74[hRluc/TK] (Promega) as an internal control. The medium was changed to DMEM with 2% FBS at 24 h after transfection. At the same time, cells were stimulated with indicated concentrations of BMP-9, and were then harvested and assayed for luciferase activity at 16 h after stimulation. Luciferase activities of the cell lysates were measured using Dual-luciferase Reporter Assay System (Promega). Results were normalized against Renilla luciferase activity.

RNA interference

Duplexes of small interfering RNA (siRNA) against human ATOH8 (Stealth RNAi Oligo IDs HSS131453, HSS131454), SMAD4 (HSS180972), and negative control (Med GC Duplex #2, Cat. 12935112) were purchased from Invitrogen (Thermo Fisher Scientific). siRNA was transfected using Lipofectamine RNAiMAX (Invitrogen, Thermo Fisher Scientific) according to the manufacturer's recommendations. The final concentration of siRNA in the culture media was 10 nM for HUVECs and 20 nM for HPAECs. The media was changed 24 h after transfection.

Microarray analysis

Microarray analysis of HUVECs with siATOH8 knock-down was performed with a GeneChip Human Genome U133 Plus 2.0 Array (Affymetrix, Thermo Fisher Scientific), essentially as described previously (58, 59). Microarray analysis of HUVECs with overexpression of ATOH8 was performed by a company (Bio Matrix Research). Microarray data of HUVECs treated with BMP ligands (GSE27661) (5), HUVECs with overexpression of Notch1 intracellular domain (GSE29850) (20), and human lung tissue obtained from 12 severe PAH patients and 11 healthy control subjects (GSE53408) (34) were retrieved from the NCBI GEO database (https://www.ncbi.nlm.nih.gov/geo/). The CEL files except for those of GSE53408 were processed using the R package *gcrma*. The CEL files of GSE53408, which use Affymetrix Human Gene 1.0 ST Array, were analyzed using R package *oligo*. If there were multiple probesets for a single gene, the maximum value among the probesets was adopted. We calculated the p-value for differential expression of each gene using moderated *t*-statistic of R package *limma*.

For fig. S1E and S1F, expressed genes with signal value more than or equal to 16 (2^4) in all conditions were analyzed. The values for ATOH8 gain-of-function (GOF) were calculated by dividing Ad-ATOH8 by Ad-LacZ, and those for loss-of-function (LOF) were calculated by dividing siControl by average of siATOH8 #1 and siATOH8 #2, both of which are positively correlated with protein abundance of ATOH8. Genes consistently regulated by ATOH8 in GOF and LOF were named “consistent genes”.

Gene set enrichment analysis (GSEA)

Gene set enrichment analysis (GSEA) was performed using the tool available at http://software.broadinstitute.org/gsea/index.jsp (60). The “consistent genes” were ranked based on the average of GOF and LOF, and the list was then used as a ranked list in the Pre-Ranked function of the GSEA software. Gene sets with a p-value < 5% and an FDR q-value < 25% were considered significant.

Chromatin immunoprecipitation (ChIP) and quantitative-PCR (ChIP-qPCR)

Chromatin isolation, sonication, immunoprecipitation using anti-SMAD1/5 antibody and quantification with real-time PCR were conducted as described previously (52). Primer sequences are given in Data File S4. The amount of immunoprecipitated DNA was calculated relative to the input.

ChIP-sequencing (ChIP-seq) and data analysis

Chromatin isolation, sonication and immunoprecipitation using anti-SMAD1/5 antibody were performed essentially as described previously (52), and were conducted in accordance with the ENCODE guidelines. Briefly, HPAECs and FLAG-ATOH8-expressing HPAECs were cultured in 100-mm plates and three to four plates (approximately $5x10^7$ cells) were used for one immunoprecipitation. Cells were fixed in 1% formaldehyde for 10 min at RT with swirling. Cross-linking was stopped by adding glycine to a final concentration of 125 mM and washing twice in ice-cold PBS. The cross-linked HPAECs were harvested by scraping, pelleted, and resuspended in 1 ml of lysis buffer containing 50 mM Tris-HCl, pH 8.0, 10 mM EDTA, 1% SDS, and cOmplete EDTA-free protease inhibitor cocktail (Roche

Applied Science). For cells stably expressing FLAG-ATOH8, we conducted nuclei isolation by NEXSON (Nuclei EXtraction by SONication) (61) with slight modifications to reduce possible non-specific binding of exogenous protein. The cross-linked cells were resuspended in 1 ml of modified Cell-Cytosolic lysis buffer containing 5 mM HEPES, pH 7.9, 85 mM KCl, 0.5% NP-40, and cOmplete EDTA-free. Cell suspensions were sonicated using a Bioruptor sonicator (Diagenode, Liège, Belgium) for 3 cycles of 15 sec ON and 30 sec OFF at 'low' power, and the nuclei were collected. For both samples, chromatin was sonicated using the Bioruptor sonicator for 3 cycles of 30 sec ON and 30 sec OFF at 'high' power, in order to shear DNA to an average fragment size of 200-500 bp. Cell extract was diluted 10-fold in ChIP dilution buffer (20 mM Tris-HCl, pH 8.0, 2 mM EDTA, 1% Triton X-100, 150 mM NaCl, cOmplete EDTA-free). One hundred and fifty μg of anti-mouse IgG Dynabeads (Invitrogen Life Technologies) were preincubated with 10 μg of antibody at 4°C overnight; chromatin was then added and was incubated at 4°C for at least another 8 h. The beads were then washed five times in RIPA buffer (50 mM HEPES-KOH, pH 7.0, 0.5 M LiCl, 1 mM EDTA, 0.7% deoxycholate, 1% NP-40) and once in TE buffer (10 mM Tris-HCl, pH 8.0, 1 mM EDTA). Immunoprecipitated samples were eluted and reverse crosslinked by incubation in elution buffer (50 mM Tris-HCl, pH 8.0, 10 mM EDTA, 1% SDS) at 65°C overnight. Genomic DNA was then extracted with a QIAquick PCR purification kit (Qiagen, Hilden, Germany).

ChIP DNA was subjected to high-throughput sequencing analysis (ChIP-seq). The libraries were constructed using IonXpress Plus Fragment Library Kit (Thermo Fisher Scientific), as described previously (62, 63). Adaptor-ligated samples were amplified by 15 cycles of PCR and purified by E-Gel SizeSelect (Thermo Fisher Scientific). Data were obtained using the Ion Proton sequencer (Thermo Fisher Scientific). Reference files of the human reference sequence assembly (NCBI Build 37/hg19, February 2009) and GTF annotation file were obtained from iGenomes (https://support.illumina.com/sequencing/sequencing_software/igenome.html). All ChIP-seq data sets were trimmed down to 50 bp and were aligned using Bowtie (version 1.1.2) (64) with the command "-S -a --best --strata -n 1 -m 1". SMAD1/5 or FLAG-ATOH8 binding regions were identified using MACS2 software (Model based analysis of ChIP-seq) (version 2.1.0) (65) with a default q-value threshold of 0.05. De novo motif prediction was performed by MEME-ChIP with a slight modification of the default settings (Maximum width: 10) (MEME-ChIP version 5.0.2; http://meme-suite.org/tools/meme-chip) (66). The logo plots were generated using the R package seqLogo.

Western blot analysis

Western blot analysis was performed essentially as described previously (5). Cells were lysed in lysis buffer containing 20 mM HEPES, pH 7.4, 100 mM NaCl, 0.5 mM EDTA, 10% glycerol, 0.2% NP40 with protease inhibitor cocktail (cOmplete, EDTA-free), or directly lysed with Laemmli sample buffer. Cytoplasmic and nuclear fractions were isolated using NE-PER Nuclear and Cytoplasmic Extraction Reagents (Pierce, Thermo Fisher Scientific) according to the recommendations of the manufacturer. Samples were separated by SDS-PAGE, blotted onto a polyvinylidene difluoride (PVDF) membrane (Pall, New York, NY, USA), and the chemiluminescence signal was detected by a luminescence image analyzer

(LAS-4000; Fujifilm, Tokyo, Japan). The intensities of the bands were quantified using ImageJ software (67).

Immunoprecipitation (IP)

HEK293T cells were transiently transfected using Lipofectamine 2000 and incubated for 36 h before analysis. Cells were lysed in a lysis buffer containing 20 mM HEPES, 100 mM NaCl, 0.5 mM EDTA, 10% glycerol, 0.2% NP-40, and cOmplete EDTA-free protease inhibitor cocktail.

FLAG-tagged protein was immunoprecipitated using anti-mouse IgG Dynabeads (Invitrogen, Thermo Fisher Scientific). Thirty μl of beads were washed once in ice cold PBS, resuspended in PBS, and preincubated with 2.5 μg of antibody on a rotating wheel at 4°C overnight, followed by two washes in PBS. Cells were lysed in the lysis buffer, and incubated with the antibody-bound Dynabeads for 4 h. Proteins in immunoprecipitates or cleared cell lysates were eluted with Laemmli sample buffer and subjected to SDS-PAGE. Western blot analysis was performed using the indicated antibodies.

To detect endogenous protein interactions, approximately $2x10^6$ of HPAEC-FLAG-ATOH8 cells (one 100-mm dish) were used for each condition. Anti-mouse IgG Dynabeads (Invitrogen, Thermo Fisher Scientific) were preincubated with 10 μg of antibody at 4°C overnight on a rotating wheel, followed by two washes with cold PBS. Cells were lysed in the lysis buffer, and incubated with the pre-treated Dynabeads for 4 h. Proteins in immunoprecipitates or cleared cell lysates were subjected to SDS-PAGE. Western blot analysis was performed using the indicated antibodies.

Statistics and reproducibility

For qRT-PCR and ChIP-qPCR, at least three independent experiments were performed and results are presented as dot plots with means. The differences between experimental groups were analyzed using Welch's *t*-test, or unequal variances *t*-test, for a single comparison, and analysis of variance (ANOVA) followed by Tukey's honestly significant difference (HSD) test for multiple comparisons. N values of experiments are provided in the figure legends, with *p <0.05, **p <0.01, and ***p <0.001 being considered significant. Western blots assays were performed at least three times with similar results.

Supplementary Material

Refer to Web version on PubMed Central for supplementary material.

Acknowledgments

We thank Dr. H. Miyoshi (RIKEN, Japan) for the lentivirus vector system; Drs. U. Engström and K. Miyazawa for anti-ATOH8 antibody production; Drs. H. Yanagisawa, A. Komuro and K. Yuki for mouse care; Dr. T. Klingström for zebrafish experiments; Drs. A. Moustakas, H. Beppu and T. Watabe for discussion; and Mss. K. Shiina, and H. Meguro for technical assistance. We also thank the SciLifeLab facility Genome Engineering Zebrafish in Uppsala for the zebrafish work.

Funding

This work was supported by a grant from Swedish Cancer Society (Grant numbers 100452 and 2016/445); KAKENHI (grants-in-aid for scientific research for Young Scientists (B) (Grant number 22790750 (DK), and for Innovative Area on Integrated Analysis and Regulation of Cellular Diversity (Grant number 17H06326 (KM)); the Global Center of Excellence Program (Integrative Life Science Based on the Study of Biosignaling Mechanisms) from the Ministry of Education, Culture, Sports, Science and Technology (MEXT), Japan; a Research Grant from the Takeda Science Foundation; European Research Council (787472); and the Swedish Research Council (2015-02757). This research was also supported by the Kanae Foundation for Research Abroad (MM), ITO Genboku and SAGARA Chian Memorial Scholarship (MM), and the Naito Foundation (DK).

References

1. Garcia de Vinuesa A, Abdelilah-Seyfried S, Knaus P, Zwijsen A, Bailly S. BMP signaling in vascular biology and dysfunction. Cytokine Growth Factor Rev. 2016; 27:65–79. [PubMed: 26823333]
2. Morrell NW, Bloch DB, ten Dijke P, Goumans MJ, Hata A, Smith J, Yu PB, Bloch KD. Targeting BMP signalling in cardiovascular disease and anaemia. Nat Rev Cardiol. 2016; 13:106–120. [PubMed: 26461965]
3. Miyazono K, Kamiya Y, Morikawa M. Bone morphogenetic protein receptors and signal transduction. J Biochem. 2010; 147:35–51. [PubMed: 19762341]
4. Morikawa M, Koinuma D, Miyazono K, Heldin CH. Genome-wide mechanisms of Smad binding. Oncogene. 2013; 32:1609–1615. [PubMed: 22614010]
5. Morikawa M, Koinuma D, Tsutsumi S, Vasilaki E, Kanki Y, Heldin CH, Aburatani H, Miyazono K. ChIP-seq reveals cell type-specific binding patterns of BMP-specific Smads and a novel binding motif. Nucleic Acids Res. 2011; 39:8712–8727. [PubMed: 21764776]
6. Moya IM, Umans L, Maas E, Pereira PN, Beets K, Francis A, Sents W, Robertson EJ, Mummery CL, Huylebroeck D, Zwijsen A. Stalk cell phenotype depends on integration of Notch and Smad1/5 signaling cascades. Dev Cell. 2012; 22:501–514. [PubMed: 22364862]
7. Skinner MK, Rawls A, Wilson-Rawls J, Roalson EH. Basic helix-loop-helix transcription factor gene family phylogenetics and nomenclature. Differentiation. 2010; 80:1–8. [PubMed: 20219281]
8. Valdimarsdottir G, Goumans MJ, Rosendahl A, Brugman M, Itoh S, Lebrin F, Sideras P, ten Dijke P. Stimulation of Id1 expression by bone morphogenetic protein is sufficient and necessary for bone morphogenetic protein-induced activation of endothelial cells. Circulation. 2002; 106:2263–2270. [PubMed: 12390958]
9. Beets K, Huylebroeck D, Moya IM, Umans L, Zwijsen A. Robustness in angiogenesis: notch and BMP shaping waves. Trends Genet. 2013; 29:140–149. [PubMed: 23279848]
10. Huertas A, Perros F, Tu L, Cohen-Kaminsky S, Montani D, Dorfmuller P, Guignabert C, Humbert M. Immune dysregulation and endothelial dysfunction in pulmonary arterial hypertension: a complex interplay. Circulation. 2014; 129:1332–1340. [PubMed: 24664216]
11. Rabinovitch M, Guignabert C, Humbert M, Nicolls MR. Inflammation and immunity in the pathogenesis of pulmonary arterial hypertension. Circ Res. 2014; 115:165–175. [PubMed: 24951765]
12. Hong KH, Lee YJ, Lee E, Park SO, Han C, Beppu H, Li E, Raizada MK, Bloch KD, Oh SP. Genetic ablation of the BMPR2 gene in pulmonary endothelium is sufficient to predispose to pulmonary arterial hypertension. Circulation. 2008; 118:722–730. [PubMed: 18663089]
13. Han C, Hong KH, Kim YH, Kim MJ, Song C, Kim MJ, Kim SJ, Raizada MK, Oh SP. SMAD1 deficiency in either endothelial or smooth muscle cells can predispose mice to pulmonary hypertension. Hypertension. 2013; 61:1044–1052. [PubMed: 23478097]
14. Diebold I, Hennigs JK, Miyagawa K, Li CG, Nickel NP, Kaschwich M, Cao A, Wang L, Reddy S, Chen PI, Nakahira K, et al. BMPR2 preserves mitochondrial function and DNA during reoxygenation to promote endothelial cell survival and reverse pulmonary hypertension. Cell Metab. 2015; 21:596–608. [PubMed: 25863249]
15. Spiekerkoetter E, Tian X, Cai J, Hopper RK, Sudheendra D, Li CG, El-Bizri N, Sawada H, Haghighat R, Chan R, Haghighat L, et al. FK506 activates BMPR2, rescues endothelial dysfunction, and reverses pulmonary hypertension. J Clin Invest. 2013; 123:3600–3613. [PubMed: 23867624]

16. Long L, Ormiston ML, Yang X, Southwood M, Graf S, Machado RD, Mueller M, Kinzel B, Yung LM, Wilkinson JM, Moore SD, et al. Selective enhancement of endothelial BMPR-II with BMP9 reverses pulmonary arterial hypertension. Nat Med. 2015; 21:777–785. [PubMed: 26076038]
17. Teichert-Kuliszewska K, Kutryk MJ, Kuliszewski MA, Karoubi G, Courtman DW, Zucco L, Granton J, Stewart DJ. Bone morphogenetic protein receptor-2 signaling promotes pulmonary arterial endothelial cell survival: implications for loss-of-function mutations in the pathogenesis of pulmonary hypertension. Circ Res. 2006; 98:209–217. [PubMed: 16357305]
18. Chowdhury HM, Sharmin N, Yuzbasioglu Baran M, Long L, Morrell NW, Trembath RC, Nasim MT. BMPRII deficiency impairs apoptosis via the BMPRII-ALK1-BclX-mediated pathway in pulmonary arterial hypertension. Hum Mol Genet. 2019; 28:2161–2173. [PubMed: 30809644]
19. Inoue C, Bae SK, Takatsuka K, Inoue T, Bessho Y, Kageyama R. Math6, a bHLH gene expressed in the developing nervous system, regulates neuronal versus glial differentiation. Genes Cells. 2001; 6:977–986. [PubMed: 11733035]
20. Chang AC, Fu Y, Garside VC, Niessen K, Chang L, Fuller M, Setiadi A, Smrz J, Kyle A, Minchinton A, Marra M, et al. Notch initiates the endothelial-to-mesenchymal transition in the atrioventricular canal through autocrine activation of soluble guanylyl cyclase. Dev Cell. 2011; 21:288–300. [PubMed: 21839921]
21. Harrington LS, Sainson RC, Williams CK, Taylor JM, Shi W, Li JL, Harris AL. Regulation of multiple angiogenic pathways by Dll4 and Notch in human umbilical vein endothelial cells. Microvasc Res. 2008; 75:144–154. [PubMed: 17692341]
22. Visel A, Minovitsky S, Dubchak I, Pennacchio LA. VISTA Enhancer Browser--a database of tissue-specific human enhancers. Nucleic Acids Res. 2007; 35:D88–92. [PubMed: 17130149]
23. Fang F, Wasserman SM, Torres-Vazquez J, Weinstein B, Cao F, Li Z, Wilson KD, Yue W, Wu JC, Xie X, Pei X. The role of Hath6, a newly identified shear-stress-responsive transcription factor, in endothelial cell differentiation and function. J Cell Sci. 2014; 127:1428–1440. [PubMed: 24463812]
24. Place ES, Smith JC. Zebrafish atoh8 mutants do not recapitulate morpholino phenotypes. PLoS ONE. 2017; 12:e0171143. [PubMed: 28182631]
25. Rawnsley DR, Xiao J, Lee JS, Liu X, Mericko-Ishizuka P, Kumar V, He J, Basu A, Lu M, Lynn FC, Pack M, et al. The transcription factor Atonal homolog 8 regulates Gata4 and Friend of Gata-2 during vertebrate development. J Biol Chem. 2013; 288:24429–24440. [PubMed: 23836893]
26. Laux DW, Febbo JA, Roman BL. Dynamic analysis of BMP-responsive smad activity in live zebrafish embryos. Dev Dyn. 2011; 240:682–694. [PubMed: 21337466]
27. Roman BL, Pham VN, Lawson ND, Kulik M, Childs S, Lekven AC, Garrity DM, Moon RT, Fishman MC, Lechleider RJ, Weinstein BM. Disruption of acvrl1 increases endothelial cell number in zebrafish cranial vessels. Development. 2002; 129:3009–3019. [PubMed: 12050147]
28. Lawson ND, Weinstein BM. In vivo imaging of embryonic vascular development using transgenic zebrafish. Dev Biol. 2002; 248:307–318. [PubMed: 12167406]
29. Siekmann AF, Lawson ND. Notch signalling limits angiogenic cell behaviour in developing zebrafish arteries. Nature. 2007; 445:781–784. [PubMed: 17259972]
30. Pardo-Martin C, Chang TY, Koo BK, Gilleland CL, Wasserman SC, Yanik MF. High-throughput in vivo vertebrate screening. Nat Methods. 2010; 7:634–636. [PubMed: 20639868]
31. Lynn FC, Sanchez L, Gomis R, German MS, Gasa R. Identification of the bHLH factor Math6 as a novel component of the embryonic pancreas transcriptional network. PLoS ONE. 2008; 3:e2430. [PubMed: 18560595]
32. Tual-Chalot S, Mahmoud M, Allinson KR, Redgrave RE, Zhai Z, Oh SP, Fruttiger M, Arthur HM. Endothelial depletion of Acvrl1 in mice leads to arteriovenous malformations associated with reduced endoglin expression. PLoS ONE. 2014; 9:e98646. [PubMed: 24896812]
33. Huang Z, Wang D, Ihida-Stansbury K, Jones PL, Martin JF. Defective pulmonary vascular remodeling in Smad8 mutant mice. Hum Mol Genet. 2009; 18:2791–2801. [PubMed: 19419974]
34. Zhao YD, Yun HZH, Peng J, Yin L, Chu L, Wu L, Michalek R, Liu M, Keshavjee S, Waddell T, Granton J, et al. De novo synthesize of bile acids in pulmonary arterial hypertension lung. Metabolomics. 2014; 10:1169–1175. [PubMed: 25374487]

35. Montagner M, Enzo E, Forcato M, Zanconato F, Parenti A, Rampazzo E, Basso G, Leo G, Rosato A, Bicciato S, Cordenonsi M, et al. SHARP1 suppresses breast cancer metastasis by promoting degradation of hypoxia-inducible factors. Nature. 2012; 487:380–384. [PubMed: 22801492]
36. Skuli N, Liu L, Runge A, Wang T, Yuan L, Patel S, Iruela-Arispe L, Simon MC, Keith B. Endothelial deletion of hypoxia-inducible factor-2α (HIF-2α) alters vascular function and tumor angiogenesis. Blood. 2009; 114:469–477. [PubMed: 19439736]
37. Skuli N, Majmundar AJ, Krock BL, Mesquita RC, Mathew LK, Quinn ZL, Runge A, Liu L, Kim MN, Liang J, Schenkel S, et al. Endothelial HIF-2α regulates murine pathological angiogenesis and revascularization processes. J Clin Invest. 2012; 122:1427–1443. [PubMed: 22426208]
38. Chen H, Shi S, Acosta L, Li W, Lu J, Bao S, Chen Z, Yang Z, Schneider MD, Chien KR, Conway SJ, et al. BMP10 is essential for maintaining cardiac growth during murine cardiogenesis. Development. 2004; 131:2219–2231. [PubMed: 15073151]
39. Brusselmans K, Compernolle V, Tjwa M, Wiesener MS, Maxwell PH, Collen D, Carmeliet P. Heterozygous deficiency of hypoxia-inducible factor-2α protects mice against pulmonary hypertension and right ventricular dysfunction during prolonged hypoxia. J Clin Invest. 2003; 111:1519–1527. [PubMed: 12750401]
40. Cowburn AS, Crosby A, Macias D, Branco C, Colaco RD, Southwood M, Toshner M, Crotty Alexander LE, Morrell NW, Chilvers ER, Johnson RS. HIF2α-arginase axis is essential for the development of pulmonary hypertension. Proc Natl Acad Sci U S A. 2016; 113:8801–8806. [PubMed: 27432976]
41. Kapitsinou PP, Rajendran G, Astleford L, Michael M, Schonfeld MP, Fields T, Shay S, French JL, West J, Haase VH. The endothelial prolyl-4-hydroxylase domain 2/hypoxia-inducible factor 2 axis regulates pulmonary artery pressure in mice. Mol Cell Biol. 2016; 36:1584–1594. [PubMed: 26976644]
42. Dai Z, Li M, Wharton J, Zhu MM, Zhao YY. Prolyl-4 hydroxylase 2 (PHD2) deficiency in endothelial cells and hematopoietic cells induces obliterative vascular remodeling and severe pulmonary arterial hypertension in mice and humans through hypoxia-inducible factor-2α. Circulation. 2016; 133:2447–2458. [PubMed: 27143681]
43. Ghosh MC, Zhang DL, Jeong SY, Kovtunovych G, Ollivierre-Wilson H, Noguchi A, Tu T, Senecal T, Robinson G, Crooks DR, Tong WH, et al. Deletion of iron regulatory protein 1 causes polycythemia and pulmonary hypertension in mice through translational derepression of HIF2α. Cell Metab. 2013; 17:271–281. [PubMed: 23395173]
44. Brentrup D, Lerch H, Jackle H, Noll M. Regulation of Drosophila wing vein patterning: net encodes a bHLH protein repressing rhomboid and is repressed by rhomboid-dependent Egfr signalling. Development. 2000; 127:4729–4741. [PubMed: 11023875]
45. Yao J, Zhou J, Liu Q, Lu D, Wang L, Qiao X, Jia W. Atoh8, a bHLH transcription factor, is required for the development of retina and skeletal muscle in zebrafish. PLoS ONE. 2010; 5:e10945. [PubMed: 20532172]
46. Sun B, Huo R, Sheng Y, Li Y, Xie X, Chen C, Liu HB, Li N, Li CB, Guo WT, Zhu JX, et al. Bone morphogenetic protein-4 mediates cardiac hypertrophy, apoptosis, and fibrosis in experimentally pathological cardiac hypertrophy. Hypertension. 2013; 61:352–360. [PubMed: 23248151]
47. Kautz L, Meynard D, Monnier A, Darnaud V, Bouvet R, Wang RH, Deng C, Vaulont S, Mosser J, Coppin H, Roth MP. Iron regulates phosphorylation of Smad1/5/8 and gene expression of Bmp6, Smad7, Id1, and Atoh8 in the mouse liver. Blood. 2008; 112:1503–1509. [PubMed: 18539898]
48. Groll M, Ditzel L, Löwe J, Stock D, Bochtler M, Bartunik HD, Huber R. Structure of 20S proteasome from yeast at 2.4 A resolution. Nature. 1997; 386:463–471. [PubMed: 9087403]
49. Semenza GL. Hypoxia-inducible factors in physiology and medicine. Cell. 2012; 148:399–408. [PubMed: 22304911]
50. Chen W, Hill H, Christie A, Kim MS, Holloman E, Pavia-Jimenez A, Homayoun F, Ma Y, Patel N, Yell P, Hao G, et al. Targeting renal cell carcinoma with a HIF-2 antagonist. Nature. 2016; 539:112–117. [PubMed: 27595394]
51. Cho H, Du X, Rizzi JP, Liberzon E, Chakraborty AA, Gao W, Carvo I, Signoretti S, Bruick RK, Josey JA, Wallace EM, et al. On-target efficacy of a HIF-2α antagonist in preclinical kidney cancer models. Nature. 2016; 539:107–111. [PubMed: 27595393]

52. Morikawa M, Koinuma D, Mizutani A, Kawasaki N, Holmborn K, Sundqvist A, Tsutsumi S, Watabe T, Aburatani H, Heldin CH, Miyazono K. BMP sustains embryonic stem cell self-renewal through distinct functions of different Krüppel-like factors. Stem Cell Reports. 2016; 6:64–73. [PubMed: 26771354]
53. Holmborn K, Habicher J, Kasza Z, Eriksson AS, Filipek-Gorniok B, Gopal S, Couchman JR, Ahlberg PE, Wiweger M, Spillmann D, Kreuger J, et al. On the roles and regulation of chondroitin sulfate and heparan sulfate in zebrafish pharyngeal cartilage morphogenesis. J Biol Chem. 2012; 287:33905–33916. [PubMed: 22869369]
54. Varshney GK, Carrington B, Pei W, Bishop K, Chen Z, Fan C, Xu L, Jones M, LaFave MC, Ledin J, Sood R, et al. A high-throughput functional genomics workflow based on CRISPR/Cas9-mediated targeted mutagenesis in zebrafish. Nat Protoc. 2016; 11:2357–2375. [PubMed: 27809318]
55. Filipek-Gorniok B, Holmborn K, Haitina T, Habicher J, Oliveira MB, Hellgren C, Eriksson I, Kjellen L, Kreuger J, Ledin J. Expression of chondroitin/dermatan sulfate glycosyltransferases during early zebrafish development. Dev Dyn. 2013; 242:964–975. [PubMed: 23703795]
56. Zudaire E, Gambardella L, Kurcz C, Vermeren S. A computational tool for quantitative analysis of vascular networks. PLoS ONE. 2011; 6:e27385. [PubMed: 22110636]
57. Arase M, Horiguchi K, Ehata S, Morikawa M, Tsutsumi S, Aburatani H, Miyazono K, Koinuma D. Transforming growth factor-β-induced lncRNA-Smad7 inhibits apoptosis of mouse breast cancer JygMC(A) cells. Cancer Sci. 2014; 105:974–982. [PubMed: 24863656]
58. Vasilaki E, Morikawa M, Koinuma D, Mizutani A, Hirano Y, Ehata S, Sundqvist A, Kawasaki N, Cedervall J, Olsson AK, Aburatani H, et al. Ras and TGF-β signaling enhance cancer progression by promoting the ΔNp63 transcriptional program. Sci Signal. 2016; 9:ra84. [PubMed: 27555661]
59. Koinuma D, Tsutsumi S, Kamimura N, Taniguchi H, Miyazawa K, Sunamura M, Imamura T, Miyazono K, Aburatani H. Chromatin immunoprecipitation on microarray analysis of Smad2/3 binding sites reveals roles of ETS1 and TFAP2A in transforming growth factor β signaling. Mol Cell Biol. 2009; 29:172–186. [PubMed: 18955504]
60. Mootha VK, Lindgren CM, Eriksson KF, Subramanian A, Sihag S, Lehar J, Puigserver P, Carlsson E, Ridderstrale M, Laurila E, Houstis N, et al. PGC-1α-responsive genes involved in oxidative phosphorylation are coordinately downregulated in human diabetes. Nat Genet. 2003; 34:267–273. [PubMed: 12808457]
61. Arrigoni L, Richter AS, Betancourt E, Bruder K, Diehl S, Manke T, Bonisch U. Standardizing chromatin research: a simple and universal method for ChIP-seq. Nucleic Acids Res. 2016; 44:e67. [PubMed: 26704968]
62. Harada M, Morikawa M, Ozawa T, Kobayashi M, Tamura Y, Takahashi K, Tanabe M, Tada K, Seto Y, Miyazono K, Koinuma D. Palbociclib enhances activin-SMAD-induced cytostasis in estrogen receptor-positive breast cancer. Cancer Sci. 2019; 110:209–220. [PubMed: 30343527]
63. Sundqvist A, Morikawa M, Ren J, Vasilaki E, Kawasaki N, Kobayashi M, Koinuma D, Aburatani H, Miyazono K, Heldin CH, van Dam H, et al. JUNB governs a feed-forward network of TGFβ signaling that aggravates breast cancer invasion. Nucleic Acids Res. 2018; 46:1180–1195. [PubMed: 29186616]
64. Langmead B, Trapnell C, Pop M, Salzberg SL. Ultrafast and memory-efficient alignment of short DNA sequences to the human genome. Genome Biol. 2009; 10:R25. [PubMed: 19261174]
65. Zhang Y, Liu T, Meyer CA, Eeckhoute J, Johnson DS, Bernstein BE, Nusbaum C, Myers RM, Brown M, Li W, Liu XS. Model-based analysis of ChIP-Seq (MACS). Genome Biol. 2008; 9:R137. [PubMed: 18798982]
66. Machanick P, Bailey TL. MEME-ChIP: motif analysis of large DNA datasets. Bioinformatics. 2011; 27:1696–1697. [PubMed: 21486936]
67. Schneider CA, Rasband WS, Eliceiri KW. NIH Image to ImageJ: 25 years of image analysis. Nat Methods. 2012; 9:671–675. [PubMed: 22930834]
68. Frazer KA, Pachter L, Poliakov A, Rubin EM, Dubchak I. VISTA: computational tools for comparative genomics. Nucleic Acids Res. 2004; 32:W273–279. [PubMed: 15215394]

Europe PMC Funders Author Manuscripts

One-sentence summary

BMP signaling induces a transcription factor that may block pulmonary arterial hypertension from developing.

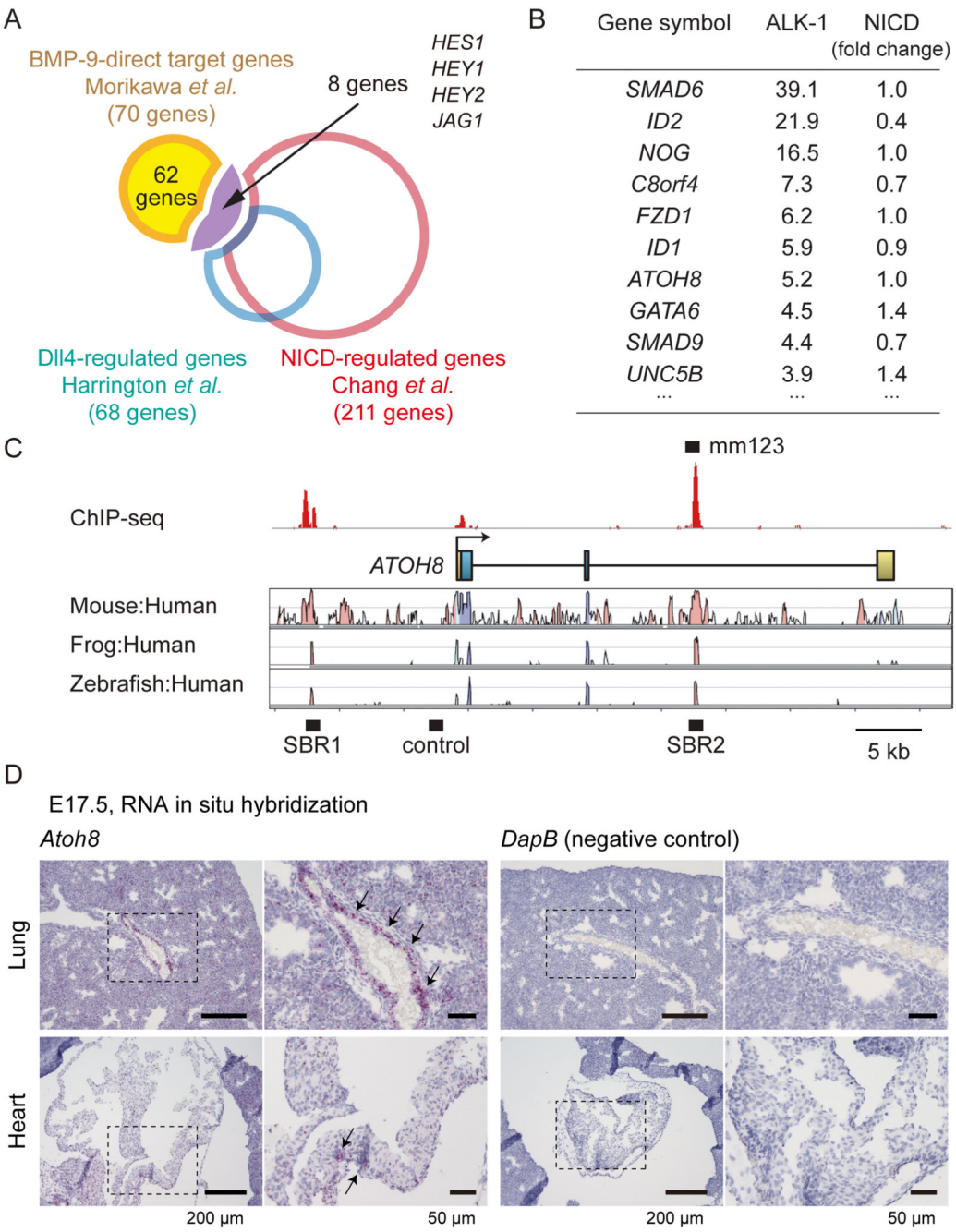

Figure 1. ATOH8 is a SMAD1/5 target gene which plays important roles in the cardiovascular system

(**A**) Overlap of genes induced by BMP-9/ALK-1 (GSE27661) (5), Notch ligand DLL4 (21) or the Notch intracellular domain (NICD) (GSE29850) (20) in human umbilical vein endothelial cells (HUVECs), illustrated by a Venn diagram.

(**B**) List of genes that are induced by ALK-1 activation, but not induced by Notch (top 10 genes are presented).

Europe PMC Funders Author Manuscripts

(**C**) Visualization of the *ATOH8* locus and the result of SMAD1/5 ChIP-seq analysis. Red peaks represent ChIP regions (top panel). The conservation plots for mouse/human, frog/human and zebrafish/human are derived from the VISTA genome browser (middle panel) (68), which presents the sequence conservation between species. SBR, Smad binding region. Control, a negative control region used in ChIP-qPCR experiment.
(**D**) ISH for the expression of mouse *Atoh8* mRNA (red dots, indicated by arrows) and control genes in the E17.5 embryo. High-magnification images of the dashed-square areas are presented. Images are representative of different experiments (more than n=3 independent samples). Scale bar: 200 μm (left) and 50 μm (right).

Europe PMC Funders Author Manuscripts

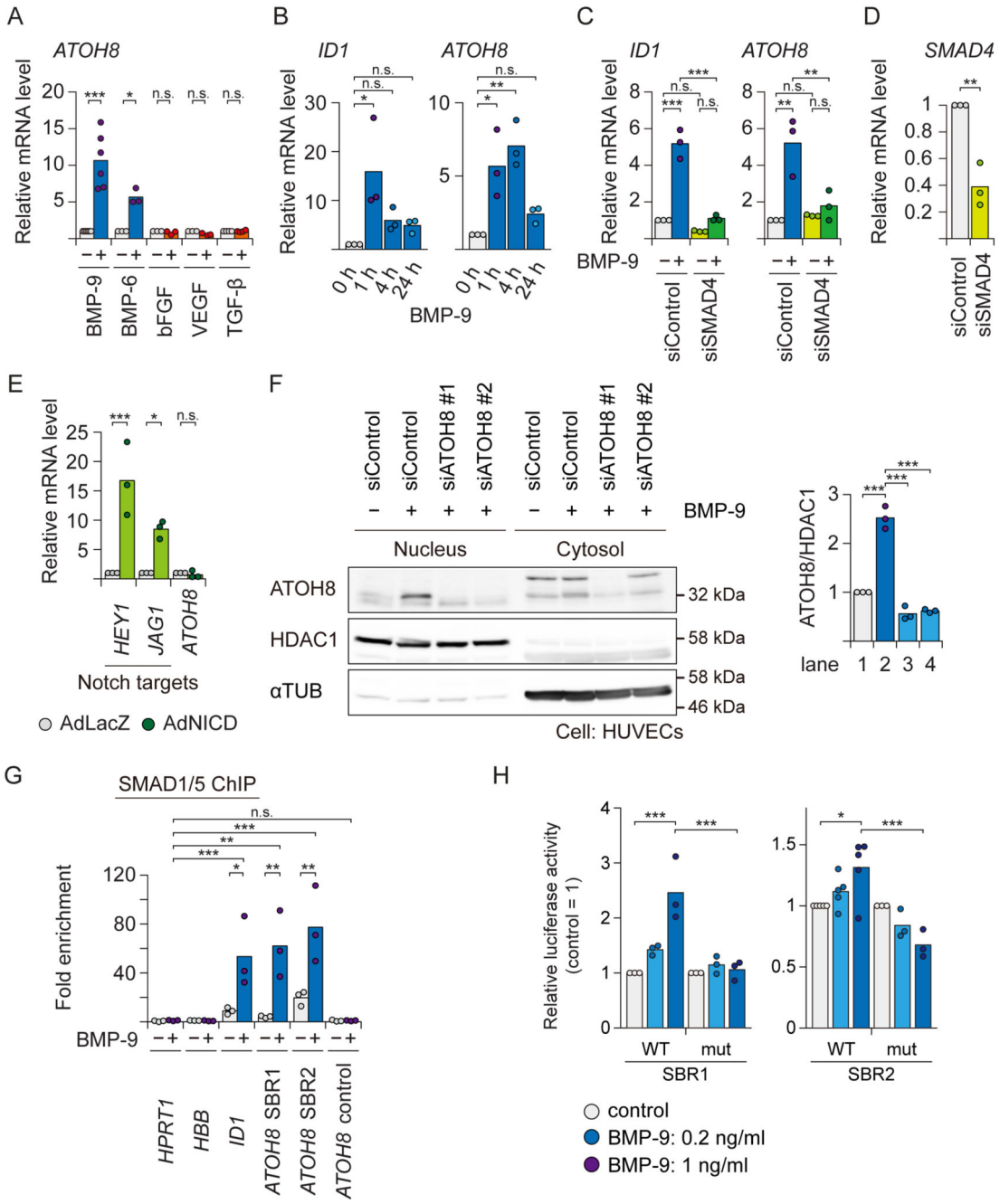

Figure 2. ATOH8 is induced by BMP-9/ALK-1 but not by Notch in ECs

(**A**) qRT-PCR analysis of HUVECs treated for 2 h with angiogenic cytokines as indicated. *GAPDH* was used as endogenous control, and data were normalized to the control condition. Results of n≥3 independent experiments are shown by scatter plots with bars representing the means.

(**B**) qRT-PCR analysis of HUVECs treated with BMP-9 (1 ng ml^{-1}) for the indicated time periods. *GAPDH* was used as endogenous control. Results of n=3 independent experiments are shown by scatter plots with bars representing the means.

(**C** and **D**) qRT-PCR analysis of HUVECs transfected with siRNA against SMAD4 (siSMAD4) or control (siControl) for 48 h, and treated with BMP-9 (1 ng ml^{-1}) as indicated for 2 h. Knock-down efficiency of SMAD4 is presented in D. Results of n=3 independent experiments are shown by scatter plots with bars presenting the means.
(**E**) qRT-PCR analysis of HUVECs infected with control (Ad-LacZ), or Notch intracellular domain (NICD)-expressing adenoviruses (Ad-NICD). *GAPDH* was used as endogenous control, and data were normalized to the control condition. Results of n=3 independent experiments are shown by scatter plots with bars representing the means.
(**F**) Western blot analysis for endogenous ATOH8 protein in HUVECs, which were transfected with siRNA against ATOH8 (siATOH8) or control (siControl), and treated with BMP-9 (1 ng ml^{-1}) for 24 h. HDAC1 (nuclear marker) and α-Tubulin (αTUB) (cytosol marker) were used as markers for cellular fraction and loading controls. Blots are representative of n=3 independent experiments. (right) Quantification of each lane of the blots. Results of n=3 independent experiments are shown by scatter plots with bars representing the means.
(**G**) SMAD1/5 ChIP-qPCR analysis of HUVECs treated with BMP-9 (1 ng ml^{-1}) for 1.5 h. ChIP was performed using antibody against SMAD1/5. The *HPRT1* gene locus was used as a negative control region and fold enrichment was calculated. Results of n=3 independent experiments are shown by scatter plots with bars representing the means.
(**H**) Luciferase reporter assay of HUVECs transfected with the indicated reporter constructs using lentiviral vector system and treated with BMP-9 (0.2 or 1 ng ml^{-1}) for 16 h. Results of n≥3 independent experiments are shown by scatter plots with bars representing the means. Differences between the conditions were analyzed by Welch's *t*-test, or unequal variances *t*-test, for a single comparison (Fig. 2D), and Tukey's honestly significant difference (HSD) test for multiple comparisons (Fig. 2A-C, 2E-H); *$p < 0.05$, **$p < 0.01$, ***$p < 0.001$.

Europe PMC Funders Author Manuscripts

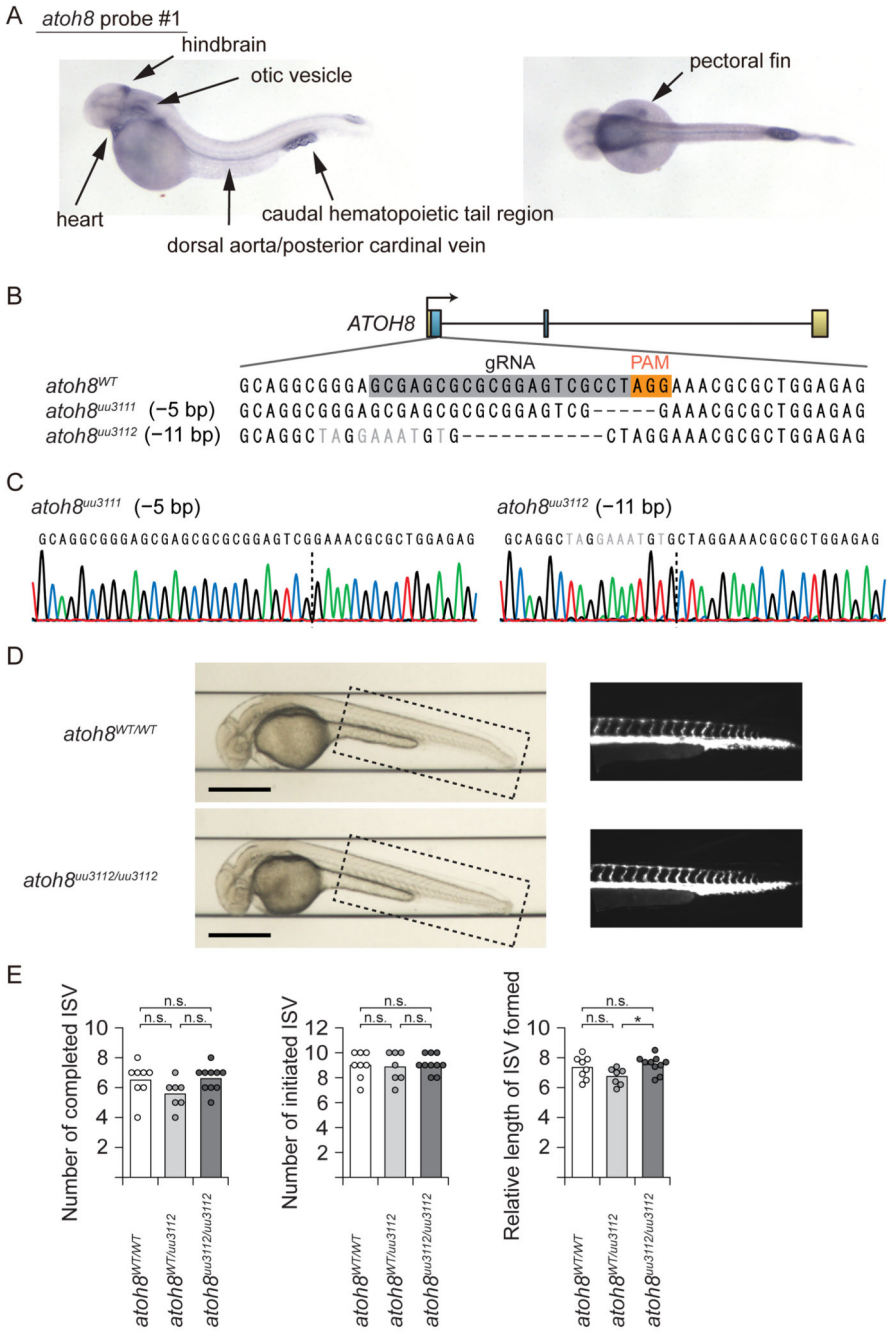

Figure 3. Zebrafish *atoh8* is expressed in large vessels but *atoh8* knockout fish display normal vascular patterning

(**A**) Whole-mount in situ hybridization of zebrafish *atoh8* at 48 hpf (hours after fertilization). (**B**) Schematic illustration of the CRISPR-Cas9/guide RNA (gRNA)-targeting sites in the exon 1 of the *atoh8* gene. The gRNA-targeting sequence is marked by a grey box and the protospacer-adjacent motif (PAM) sequence by an orange box in the wild-type sequence. The sequence of 2 mutant lines is also shown.

(**C**) Results of Sanger sequencing of genomic DNA from the mutants are presented. Dashed lines represent the deletion location.
(**D**) Representative bright field (left) and fluorescence images (right, the dashed-square area of the bright-field image) of *atoh8*$^{WT/WT}$ and *atoh8*$^{uu3112/uu3112}$ fish at 36 hpf are shown. Scale bar: 500 μm.
(**E**) Assessment of ISV formation in *atoh8*$^{WT/WT}$, and *atoh8*$^{WT/uu3112}$ and *atoh8*$^{uu3112/uu3112}$ fish at 36 hpf (n=8 for *atoh8*$^{WT/WT}$, n=7 for *atoh8*$^{WT/uu3112}$, n=10 for *atoh8*$^{uu3112/uu3112}$). Differences between the conditions were analyzed by Tukey's HSD test corrected for multiple comparisons; *$p < 0.05$.

Europe PMC Funders Author Manuscripts

Europe PMC Funders Author Manuscripts

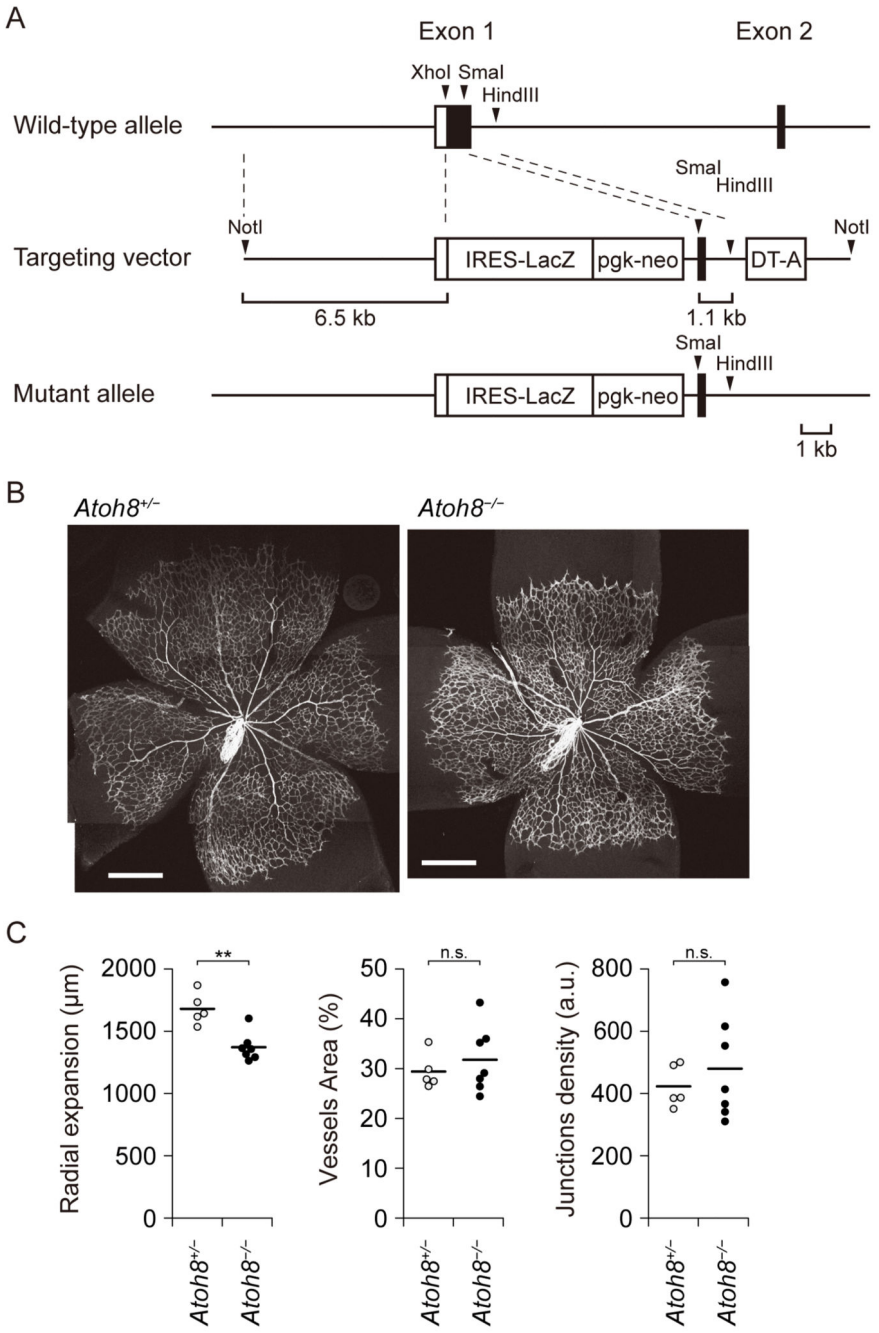

Figure 4. Loss of *Atoh8* results in a delay in retinal angiogenesis in *Atoh8*-deficient mice

(**A**) Schematic presentation of *Atoh8* wild-type (WT) allele, the targeting vector and the *Atoh8* mutant allele.

(**B**) Representative images of whole-mount retinas of P5 $Atoh8^{+/-}$ and $Atoh8^{-/-}$ mice. The tiling images were manually merged. Scale bar: 500 μm.

(**C**) Bar graphs show the mean distance of radial expansion, vessel area, and junction density of $Atoh8^{+/-}$ and $Atoh8^{-/-}$ mice. The data are presented as dot plot (n=5 and 7 mice,

respectively), and differences between the conditions were analyzed by Welch's *t*-test; **p < 0.01.

Europe PMC Funders Author Manuscripts

Europe PMC Funders Author Manuscripts

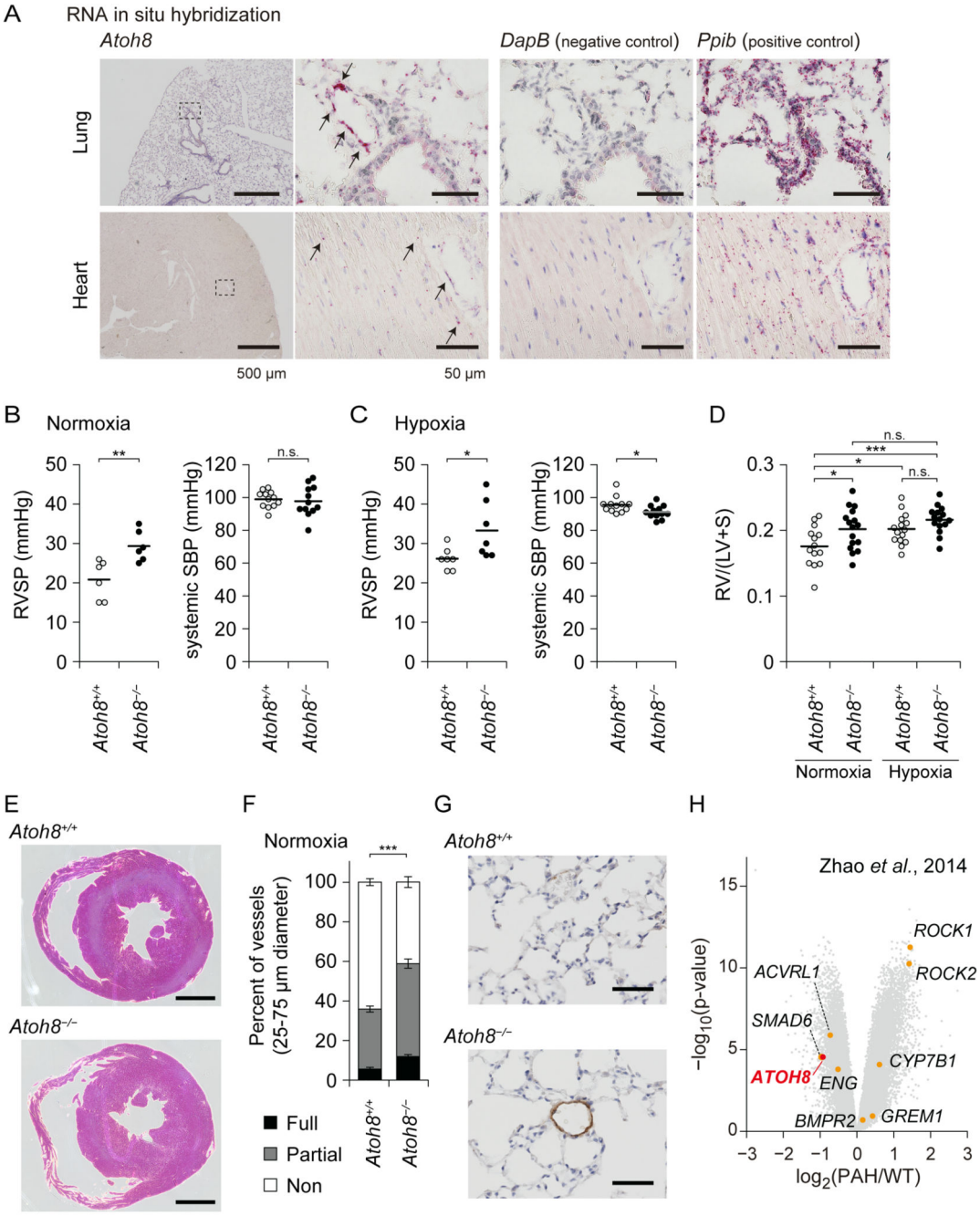

Figure 5. *Atoh8*-deficient mice exhibit a phenotype resembling human PAH

(A) ISH for expression of mouse *Atoh8* mRNA (red dots, indicated by arrows) and control genes in the lungs and hearts of aged mice in normoxic condition. High-magnification images of the dashed-square areas are presented. Images are representative of different experiments (more than n=3 independent samples), Scale bar: 500 μm (left) and 50 μm (right three panels).

(**B** and **C**) Assessment of right ventricular systolic pressure (RVSP) and systemic systolic blood pressure (SBP) of *Atoh8*$^{-/-}$ mice. RVSP was measured in normoxic (B) and hypoxic

(C) conditions. The data are presented as scatter plot with mean (RVSP: n=6 for each group in normoxia and n=7 in hypoxia, systemic SBP: n=12), and differences between the conditions were analyzed by Welch's *t*-test; **p < 0.01.

(**D** and **E**) Assessment of right ventricular hypertrophy of *Atoh8*$^{-/-}$ mice. The hearts of *Atoh8*$^{+/+}$ and *Atoh8*$^{-/-}$ male mice in the normoxic and hypoxic conditions were analyzed (n=14 *Atoh8*$^{+/+}$ mice under normoxia, n=16 *Atoh8*$^{-/-}$ mice under normoxia, n=15 mice for each genotype under hypoxia). The data are presented as scatter plot with mean (D). Representative images of hearts of mice in normoxia are presented (E). Differences between the conditions were analyzed by Tukey's HSD test corrected for multiple comparisons; *p < 0.05, ***p < 0.001. Scale bar: 1 mm.

(**F** and **G**) Assessment of pulmonary arterial muscularization of *Atoh8*$^{-/-}$ mice. Non-, partially and fully muscularized arteries, as a percentage of total alveolar wall and duct arteries, were scored in *Atoh8*$^{+/+}$ (n=17) and *Atoh8*$^{-/-}$ (n=19) male mice. The data is presented as a stacked bar plot, mean ± SEM (F), and representative images of immunohistochemical staining for smooth muscle α-actin are shown (G). Scale bars, 50 μm. Welch's *t*-test for fully muscularized vessels; ***p < 0.001.

(**H**) Volcano plot of differentially expressed genes from PAH patients (n=12) and healthy control subjects (n=11) (GSE53408) (34).

Europe PMC Funders Author Manuscripts

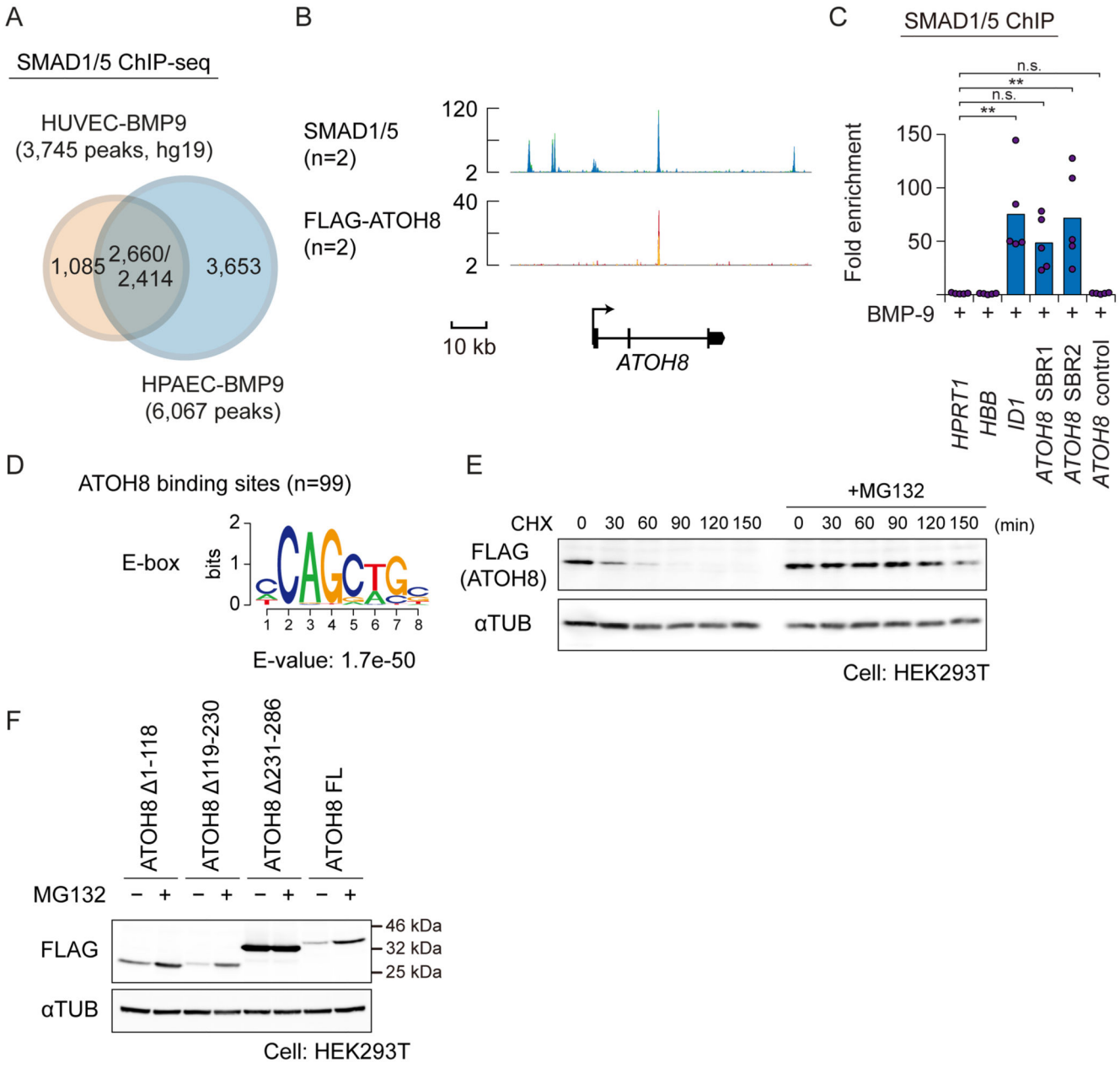

Figure 6. ATOH8 does not function as a DNA-binding factor in HPAECs

(**A**) A Venn diagram indicating overlap of SMAD1/5 binding sites of HUVECs (5) and HPAECs treated with BMP-9. The numbers of overlapping regions are not identical, because some of the peaks do not show a one-by-one correspondence.

(**B**) Visualization of the *ATOH8* gene locus and the result of SMAD1/5 (n=2) and FLAG-ATOH8 (n=2) ChIP-seq in HPAECs. Colored peaks represent ChIP regions (top panel).

(**C**) SMAD1/5 ChIP-qPCR analysis of HPAECs treated with BMP-9 (1 ng ml^{-1}) for 1.5 h. ChIP was performed using antibody against SMAD1/5. The *HPRT1* gene locus was used as a negative control region, and fold enrichment was calculated. Results of n=5 independent experiments are shown by scatter plots with bars representing the means. Differences

between the conditions were analyzed by Tukey's HSD test corrected for multiple comparisons; *p < 0.05.

(**D**) De novo motif prediction analysis of the FLAG-ATOH8 binding sites.

(**E**) Western blot analysis of FLAG-tagged ATOH8 protein expression in HEK293T cells, cultured with or without 10 μM MG132 for 16 h and then treated with 100 μg/ml cycloheximide (CHX) for indicated time periods. αTUB was used as a loading control. Blots are representative of n=3 independent experiments.

(**F**) Western blot analysis of FLAG-tagged ATOH8 protein in HEK293T cells. Cells were transfected with indicated ATOH8 mutants (0.3 μg for Δ231−286, and 1 μg for the others). Twenty-four hours after transfection, cells were incubated with or without 10 μM MG132 for 16 h. Cells were then lysed and subjected to SDS-PAGE and Western blotting. αTUB was used as a loading control. Blots are representative of n=3 independent experiments. FL, full-length.

Europe PMC Funders Author Manuscripts

Europe PMC Funders Author Manuscripts

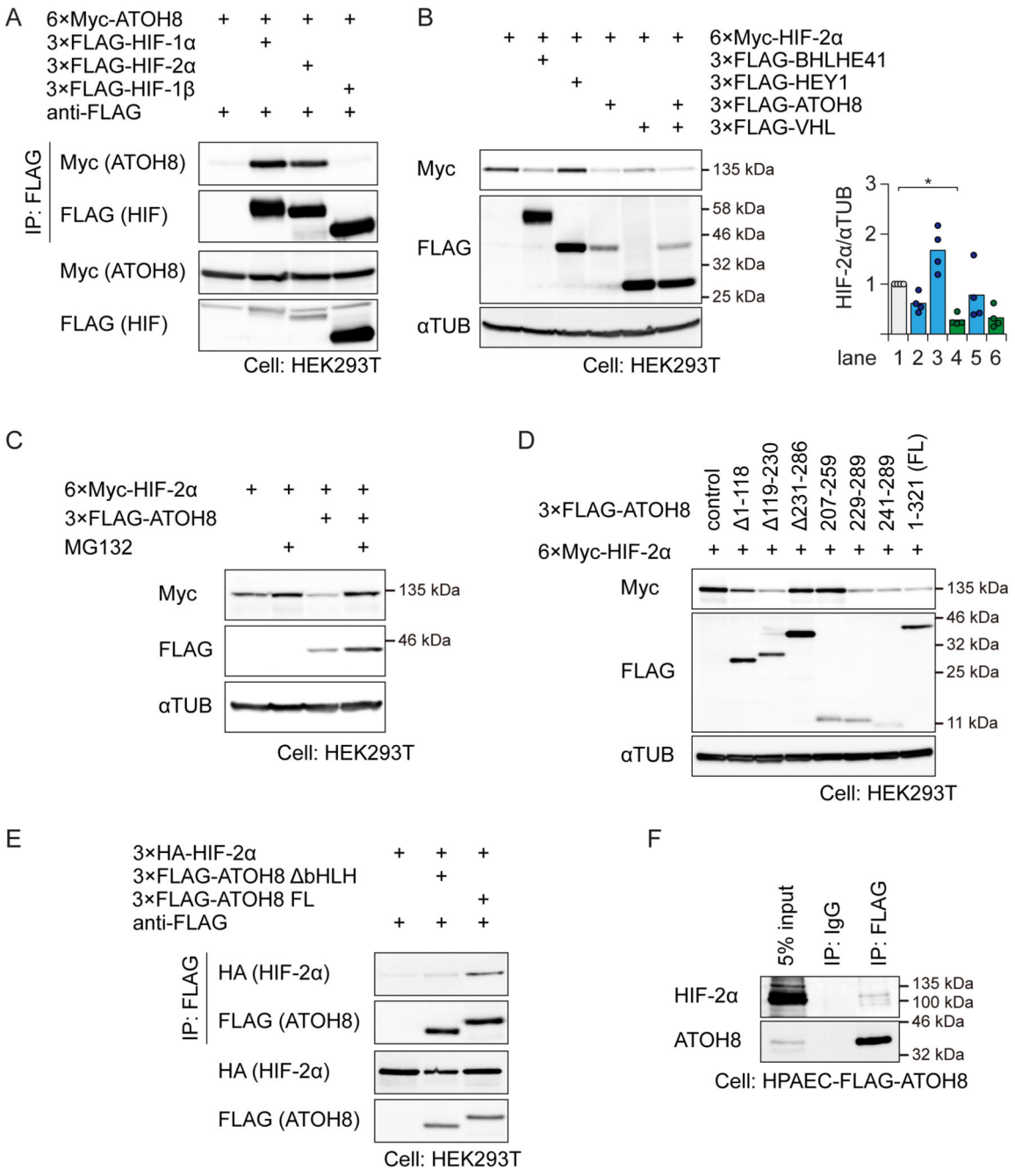

Figure 7. ATOH8 physically interacts with HIF-2α and decreases its abundance

(**A**) HEK293T cells were transiently transfected with the indicated plasmids. FLAG immunoprecipitates (IP) were subjected to Western blotting for FLAG (to detect HIF-1α or HIF-2α) or Myc (to detect ATOH8). Blots are representative of n=3 independent experiments.

(**B**) HEK293T cells were transfected with the indicated plasmids and subjected to Western blotting to assess the effect of ATOH8 coexpression on HIF-2α abundance. αTUB was used as a loading control. Blots are representative of n=4 independent experiments. (right)

Quantification of each lane of the blots. Results of n=4 independent experiments are shown by scatter plots with bars representing the means. Differences between the conditions were analyzed by Tukey's HSD test corrected for multiple comparisons; *$p < 0.05$.

(**C**) HEK293T cells were transfected with the indicated plasmids, treated with MG132, and subjected to Western blotting to assess proteasomal inhibition modulates the effect of ATOH8 coexpression on HIF-2α abundance. αTUB was used as a loading control. Representative images are taken from n≥3 experiments.

(**D**) HEK293T cells were transfected with the indicated plasmids and subjected to Western blotting to determine the binding site of HIF-2α on ATOH8. αTUB was used as a loading control. Blots are representative of n=3 independent experiments. See also Fig. S5A.

(**E**) FLAG immunoprecipitates were subjected to Western blotting to assess the requirement for the bHLH domain of ATOH8 on the ATOH8/HIF-2α interaction. Blots are representative of n=3 independent experiments.

(**F**) HPAECs stably expressing FLAG-ATOH8 were maintained under hypoxic conditions (≤1% O_2) for 24 h. FLAG immunoprecipitates were subjected to Western blotting for FLAG (to detect HIF-1α or HIF-2α) or Myc (to detect ATOH8). Blots are representative of n=3 independent experiments.

Europe PMC Funders Author Manuscripts

Europe PMC Funders Author Manuscripts

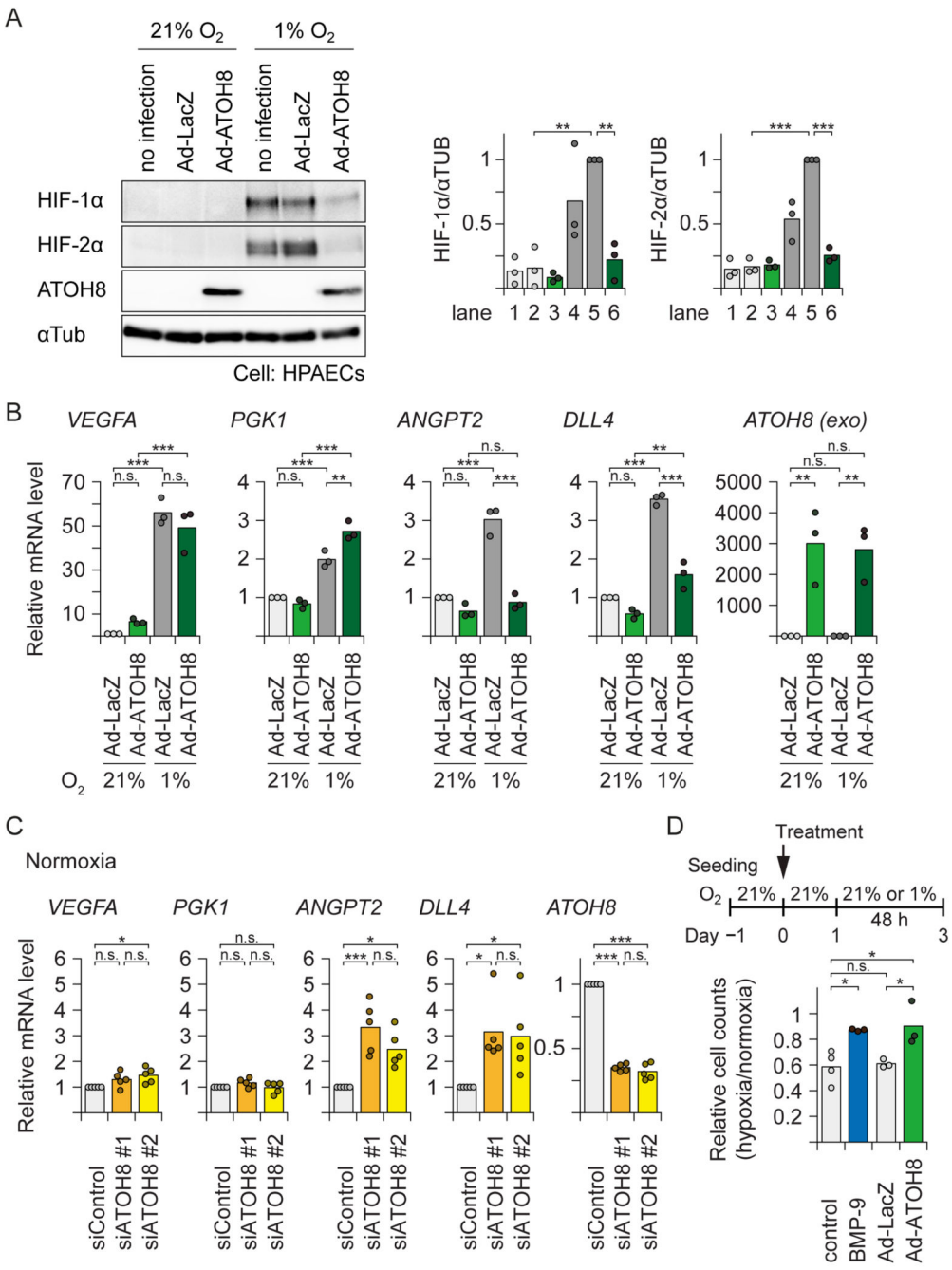

Figure 8. ATOH8 attenuates hypoxia-induced HIF-2α activation and target gene expression

(**A**) HPAECs were infected with either Ad-ATOH8 or control (Ad-LacZ) for 24 h, then transferred to hypoxic (≤1% O_2) or normal (21% O_2) conditions for an additional 24 h. Cell lysates were analysed by Western blotting for endogenous HIF proteins. αTUB was used as a loading control. Blots are representative of n=3 independent experiments. (right) Quantification of each lane of the blots. Results of n=3 independent experiments are shown by a scatter plot with bar presenting the means. Differences between the lanes were analyzed by Tukey's HSD test corrected for multiple comparisons; **p < 0.01, ***p < 0.001.

(**B**) qRT-PCR analysis of HPAECs infected with either Ad-ATOH8 or control (Ad-LacZ) for 24 h, then transferred to hypoxic (≤1% O_2) or normal (21% O_2) conditions for an additional 24 h. *HPRT1* was used as endogenous control and data were normalized to the control condition. Results of n=3 independent experiments are shown by a scatter plot with bar representing the means. exo: exogenous. Differences between the conditions were analyzed by Tukey's HSD test corrected for multiple comparisons; **p < 0.01, ***p < 0.001.
(**C**) qRT-PCR analysis of HPAECs transfected with either siRNAs specific for ATOH8 or control siRNA for 60 h. *HPRT1* was used as endogenous control, and data were normalized to the control condition. Results of n=5 independent experiments are shown by a scatter plot with bar representing the means. Differences between the conditions were analyzed by Tukey's HSD test corrected for multiple comparisons; *p < 0.05, ***p < 0.001.
(**D**) HPAECs were seeded 24 h before treatment. Cells were treated with BMP-9 (5 ng ml^{-1}) or infected with either Ad-ATOH8 or control (Ad-LacZ) for 24 h, then transferred to hypoxic (≤1% O_2) or normal (21% O_2) conditions for an additional 48 h. The ratio of the number of the cells under hypoxia to that under normoxia was calculated. Results of n≥3 independent experiments are shown by a scatter plot with bar representing the means. Differences between the conditions were analyzed by Tukey's HSD test corrected for multiple comparisons; *p < 0.05.